



# Structural setting of the Young-Davidson syenite-hosted gold deposit in the Western Cadillac-Larder Lake Deformation Zone, Abitibi Greenstone Belt, Superior Province, Ontario



Jian Zhang<sup>a,b</sup>, Shoufa Lin<sup>b,\*</sup>, Robert Linnen<sup>c</sup>, Ryan Martin<sup>b</sup>

<sup>a</sup> Earth System Science Programme, The Chinese University of Hong Kong, Hong Kong

<sup>b</sup> Department of Earth and Environmental Sciences, University of Waterloo, Waterloo, Ontario, N2L 3G1, Canada

<sup>c</sup> Department of Earth Sciences, Western University, Ontario, N6A 5B7, Canada

## ARTICLE INFO

### Article history:

Received 3 September 2013

Received in revised form 21 March 2014

Accepted 3 April 2014

Available online 13 April 2014

### Keywords:

Archean

Superior Province

Cadillac – Larder Lake Deformation Zone

Structures

Syenite

Gold Mineralization

## ABSTRACT

Within the southern Abitibi greenstone belt of the Superior Province, intrusion-related, in particular syenite-hosted gold deposits represent a significant type that is poorly understood. Whether the gold mineralization is genetically linked to the syenite intrusions (as in a magmatic model) or structurally associated with the development of subsequent shear zones remains very controversial. Our new structural data show that the multiply deformed Young-Davidson gold deposit and its surrounding Matachewan area occur along the western extension of the Cadillac – Larder Lake Deformation Zone (CLLDZ), a tectonically and economically important crustal-scale deformation zone in the southern Abitibi greenstone belt. Four generations ( $D_1$ – $D_4$ ) of deformation are recognized. The first part of the  $D_1$  deformation ( $D_{1a}$ ) records a NE-SW-oriented shortening and resulted in regional upright folding without penetrative foliation, whereas the subsequent  $D_{1b}$  generates regional penetrative foliations and top-to-NE reverse faults.  $D_2$  occurs during a NW-SE-oriented shortening and produces asymmetric folds, oblique-slip thrusts and dextral strike-slip shear zones.  $D_3$  semi-brittle deformation refolds the  $D_1$  and  $D_2$  fabrics, whereas the latest  $D_4$  sinistral fault records a Paleoproterozoic brittle deformation.

The Young-Davidson deposit is a lode-gold deposit that at least in part was structurally controlled. It is associated with the development of the CLLDZ and hosted in a syenite. Four main generations of veins are identified in the syenite.  $V_1$  veins are characterized by folded and boudinaged quartz–ankerite veins,  $V_2$  veins are represented by folded or en echelon quartz–pyrite veinlets,  $V_3$  veins are comprised of en echelon quartz–carbonate veins with sulfide minerals, and  $V_4$  veins consist of planar carbonate–quartz veins and minor hematite. Petrological studies reveal that the major phase of gold mineralization is associated with the  $V_2$  veins and partially with the  $V_3$  veins. Gold mineralization and emplacement of the associated veins appear to have occurred during regional  $D_{1b}$  NE-SW-oriented shortening and top-to-NE shearing and the syenite acted as a mechanical trap due to competency contrast to the wall rock

© 2014 Elsevier B.V. All rights reserved.

## 1. Introduction

The Cadillac – Larder Lake Deformation Zone (CLLDZ) is considered as one of the most important crustal-scale structures in the Abitibi greenstone belt (Fig. 1). It is well known for its lithological complexity, polyphase deformation, pervasive hydrothermal alteration, and spatial association with world-class orogenic gold deposits (Fig. 1; Lovell, 1967; Ludden et al., 1986; Card et al., 1989; Card, 1990; Poulsen et al., 1992, 2000; Wilkinson et al., 1999;

Robert, 2001a,b; Ayer et al., 2002). In order to better understand the relationships between deformation and gold mineralization, extensive structural investigations have been carried out over the CLLDZ in the last few decades and have established diverse kinematic models (e.g. Hodgson and Hamilton, 1989; Hodgson et al., 1991; Smith et al., 1993; Robert, 1989, 2001a; Wilkinson et al., 1999; Ispolatov et al., 2005, 2008). Among these models, however, the origin of felsic intrusion-related, in particular syenite-hosted gold deposits is still poorly constrained. Whether the gold mineralization is genetically linked to the syenite intrusion (as in a magmatic model) or structurally associated with the development of subsequent shear zone remains controversial (e.g. Colvine, 1989; Mason and Helmstaedt, 1992; Corfu, 1993). A complicating factor is that

\* Corresponding author. Tel.: +1 519 888 4567x36557.

E-mail address: [shoufa@uwaterloo.ca](mailto:shoufa@uwaterloo.ca) (S. Lin).

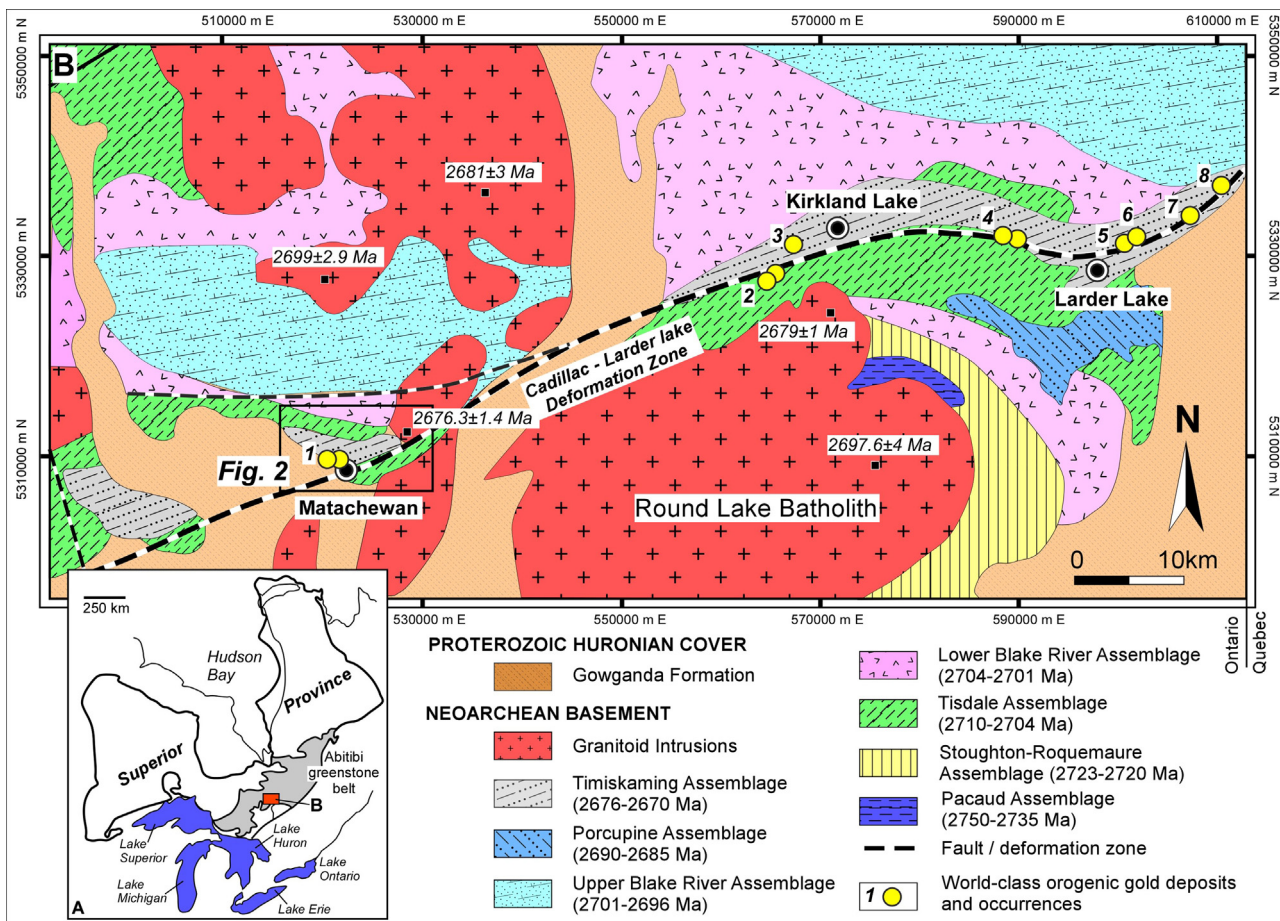


**Fig. 1.** Geological map of the Cadillac – Larder Lake Deformation Zone, southern Abitibi greenstone belt (*modified after Ayer et al., 2002, 2005*). Published ages of granitoid intrusions are also shown on the map. Selected world-class orogenic gold deposits: 1 – Young-Davidson; 2 – Golden Gate; 3 – Kirkland Lake; 4 – McBean; 5 – Omega; 6 – Fernland; 7 – Baber-Larder; 8 – Kerr Addison-Chesterville.

the syenite intrusions commonly contain a large amount of inherited zircons and show a big age range that overlaps the timing of the gold mineralization (Robert, 2001b; Ayer et al., 2005). Therefore, a systematic structural study on key areas of the CLLDZ with syenite-hosted gold deposits is of significant interests to resolve this controversy.

The Matachewan area is located far west to the previously recognized CLLDZ (Fig. 1; e.g. Larder Lake, Hamilton and Hodgson, 1984; Kirkland Lake, Hodgson et al., 1991; Wilkinson et al., 1999; Val d'Or, Robert, 1989; Desrochers and Hubert, 1996; Olivo et al., 2006). Previous studies proposed that the Matachewan area contains variable scales of syenite plutons and has experienced multiple generations of deformation (Powell and Hodgson, 1992; Berger and Préfontaine, 2005). Whether the Matachewan area is a western extension of the CLLDZ is of significant importance into understanding the tectonic evolution of the southern Abitibi greenstone belt and the genesis of the orogenic gold deposits. If the Matachewan area belongs to part of the CLLDZ, the crustal-scale CLLDZ is evidenced to have extended farther west to a larger region and yields both of tectonic and economic significance. However, this issue still remains very poorly constrained due to insufficient structural and kinematic data in this area.

Located in the central part of the Matachewan area, the Young-Davidson deposit is associated with a syenite intrusion and most of the gold mineralization is contained within the intrusion, although mineralization zone also extends into the host mafic volcanic and Timiskaming metasedimentary rocks (Lovell, 1967; Sinclair, 1982; Fig. 2; also see the text below). Previous studies

surrounding the genesis of Young-Davidson gold deposit are controversial. Sinclair (1982) and Robert (2001b) suggest that the gold mineralization is temporally and genetically related to the syenite, although they have been overprinted by subsequent regional folding and related penetrative cleavage. In contrast, recent investigation on mine-scale surface outcrops suggests a post-intrusion, structural control of gold mineralization (D. Rhys, 2003, unpublished report). Based on more recent geological mapping, Berger and Préfontaine (2005) interpreted that the second generation of deformational fabrics (e.g. L<sub>2</sub> lineations), which are parallel to the plunge of F<sub>2</sub> folds, locally controls the gold mineralization. The multiple generations of deformational superposition and their intimately spatial relationships to the gold mineralization therefore make the Matachewan area and its syenite-hosted Young-Davidson deposit as the most promising areas for this study.

To resolve the above controversies, a three-year (2008–2010) multidisciplinary research project was carried out in the Matachewan area. The work reported here mainly comprises the structural component of the project. In this work, extensive surface and underground mapping (at scales ranging from 1:15,000 to 1:100) are combined with detailed analysis of different generations of structures at variable scales. In this paper, major lithology and overall deformational history of the Matachewan area are first presented, with emphasis on key deformational stages and their structural features that are correlated to the large-scale CLLDZ. This is followed by a detailed analysis of multiple stages of auriferous veining system within the Young-Davidson syenite intrusion with

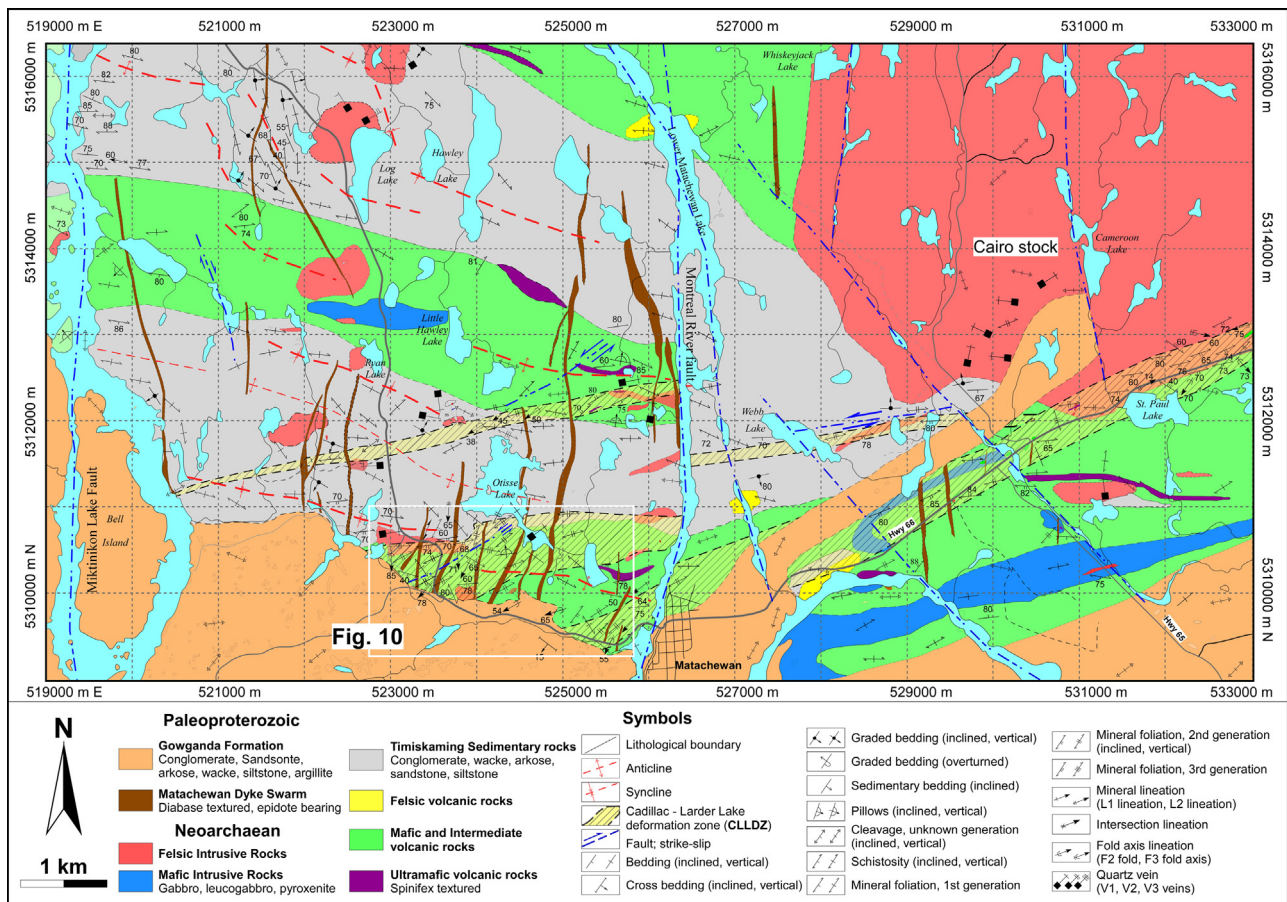


**Fig. 2.** Detailed geological map of the Matachewan area, showing distributions of major lithology, different generations of structures and high strain zones related to the CLLDZ.

respect to magmatism, deformation, alteration and mineralization. The results of this paper provide solid evidence that the Young-Davidson deposit and its surrounding area are a western extension of the CLLDZ. Systematic structural data are used to decipher the structural setting of the syenite intrusion and the spatially associated gold mineralization, and to further test the controversial genetic models.

## 2. Regional geology

The Matachewan area, as used in this paper, refers to an area approximately 70 km southwest of Kirkland Lake, and covers eastern part of the Powell and western part of the Cairo Townships, with the UTM co-ordinates (NAD 83, Zone 17) of 519000E–533000E and 5309000N–5316000N, respectively (Fig. 1). Similar to other parts of the southern Abitibi greenstone belt, this area comprises Neoarchean rock assemblages ranging from ultramafic to mafic volcanics, intermediate to felsic volcanics, alkalic intrusions and Timiskaming Group metasedimentary rocks that are extensively metamorphosed up to greenschist facies (Lovell, 1967; Powell, 1991; Berger and Préfontaine, 2005). The Neoarchean rock assemblages are pervasively intruded and crosscut by the Paleoproterozoic (~2470 Ma) N-S-trending Matachewan dike swarm (Heaman, 1997), all of which are unconformably overlain by the Gowganda Formation of the Cobalt Group of the Paleoproterozoic Huronian Supergroup. The Cobalt Group is intruded by the ~2219 Ma Nipissing dyke swarm, which is the youngest rock of this area (Powell and Hodgson, 1992). Both the Neoarchean rock assemblages and CLLDZ are horizontally offset by the Proterozoic

N-S-trending Mistinikon Lake fault and Montreal River fault (Fig. 2; Powell, 1991).

### 2.1. Tisdale assemblage

The oldest and dominant lithology of the Matachewan area is the Tisdale assemblage with an age of 2710–2704 Ma (Ayer et al., 2005). It consists of ultramafic, mafic and intermediate to felsic volcanic rocks. The ultramafic rocks are characterized by pillowed and spinifex-textured komatiites (Fig. 3A). They occur as thin layers and are locally in tectonic contact with the Timiskaming metasedimentary rocks (Fig. 2). In some places the ultramafic volcanic rocks were intruded by syenite intrusions, indicating that the syenite is younger (Linnen et al., 2012). Mafic volcanic rocks are composed of massive flows, variolitic flows, brecciated flows and basaltic pillows, metamorphosed to sub- to greenschist facies. These rocks occur in three separate, approximately WNW-trending bands (green in color), which are intercalated with two sedimentary rock bands of the Timiskaming assemblage (grey in color; Fig. 2). This repetition of stratigraphy is a consequence of isoclinal upright folding ( $D_{1a}$  below). The northern and middle bands are located outside of the CLLDZ in contrast to the southern band, where most of the mafic volcanic rocks are located within the CLLDZ and experienced intense deformation and associated chlorite-sericite-carbonate-magnetite alteration. Pillowed flows outcrop mainly on the Young-Davidson mine property and are generally flattened and folded to form the regional foliations (Fig. 3B). At the southern boundary of the southern band, mafic volcanic rocks are unconformably overlain by the

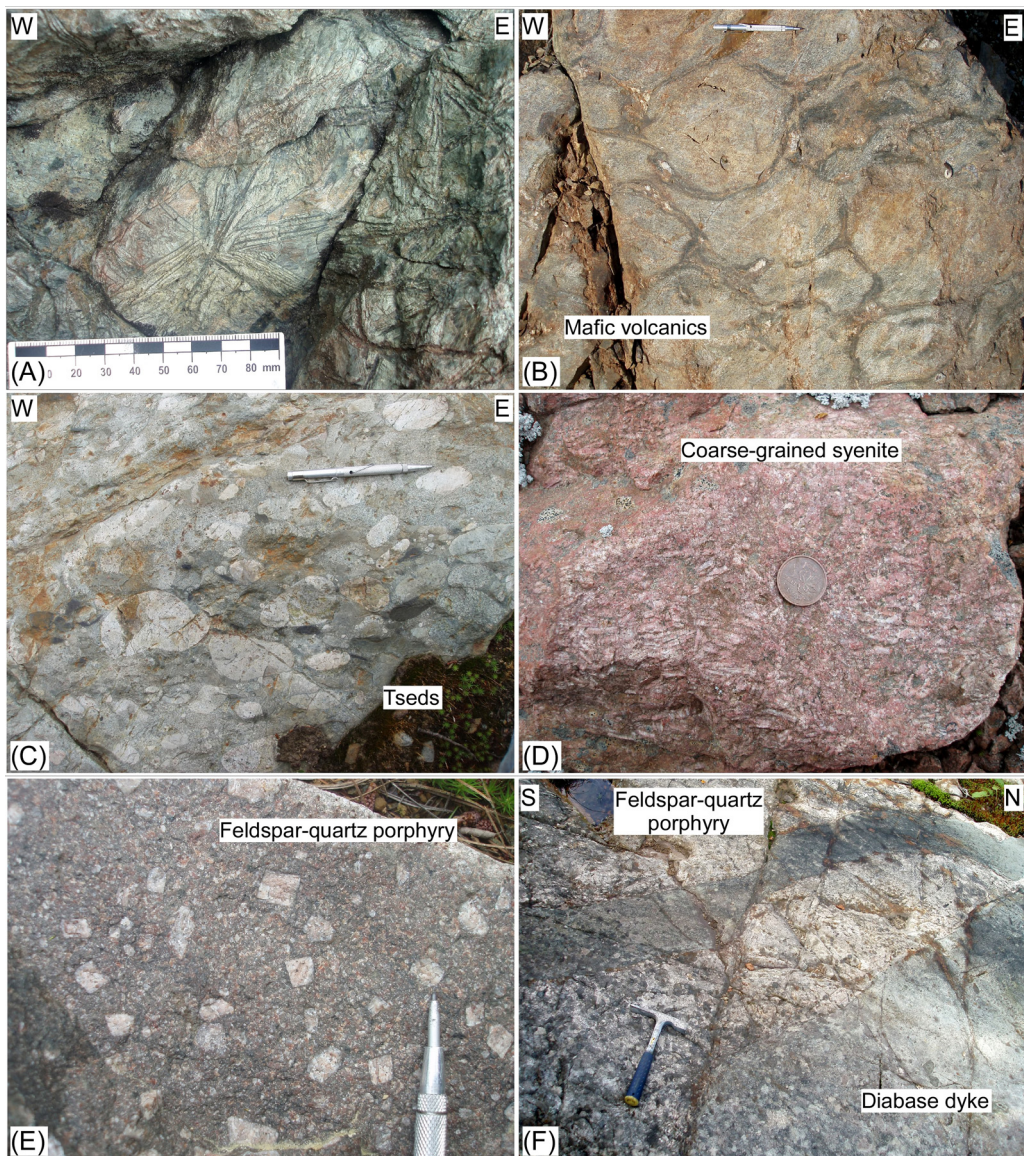


**Fig. 3.** Field photos of representative lithology of the Matachewan area. All photos show sub-horizontal surfaces. (A) Ultramafic volcanic rocks (komatiites) with characteristic spinifex texture. (B) Weakly deformed pillow basalt. (C) Weakly deformed Timiskaming conglomerate. (D) Coarse-grained 'trachytic textured' syenite of the Young-Davidson deposit. (E) Feldspar-quartz porphyry. (F) Paleoproterozoic diabase dykes intruding the feldspar-quartz porphyry.

Proterozoic Gowganda Formation (Fig. 2; Berger and Préfontaine, 2005).

Intermediate to felsic volcanic rocks are sporadically distributed in this area, consisting of lapilli tuff, tuff breccia, massive flow of rhyolite (extrusive rocks) and fine-grained aplite (Fig. 2; Linnen et al., 2012). The intermediate and felsic volcanic rocks have been considered as the upper part or younger phase of the Tisdale assemblage (Ayer et al., 2002).

## 2.2. Timiskaming assemblage

The Timiskaming metasedimentary rock assemblage is considered to be the youngest supracrustal unit of the southern Abitibi greenstone belt (2676–2670 Ma; Fig. 2; Ayer et al., 2002, 2005), overlying unconformably the older volcanic rocks of the Tisdale assemblage. It consists of fine- to coarse-grained sandstone, wacke, chert, siltstone, and polymictic conglomerate deposited in alluvial and fluvial environments (Mueller et al., 1994; Ayer et al., 2002). As indicated above, the Timiskaming assemblage occurs in two bands,

intercalated with mafic volcanic rocks of the Tisdale Assemblage (Fig. 2; Berger, 2006). Clasts in the conglomerate range from 0.5 to 15 cm in length and are extensively flattened and elongated parallel to the regional S<sub>1b</sub> penetrative foliation (Fig. 3C). The well sorted greywacke and sandstone show good younging structures such as cross-bedding and graded bedding (see below).

Within the Timiskaming assemblage, a distinct and thin unit of syenite boulder conglomerate occurs along the southern margin of the Cairo syenite (Berger, 2006; Fig. 2). Petrological and geochronological data revealed an intimate relationship between the boulder and the Cairo syenite, which indicates that the emplacement of the syenite intrusions and deposition of the Timiskaming assemblage were broadly coeval (Berger, 2006; Linnen et al., 2012).

## 2.3. Syenite intrusions

Syenite intrusions include syenite, syenite porphyry, and mafic syenite. In addition, lamprophyre dykes crosscut syenite. The syenites occur as dikes, sills and small to large plutons (Fig. 2). Syenite

is pinkish red in color and shows coarse- to medium-grained equigranular textures (locally with a trachytic texture) with massive structures (Fig. 3D). It is composed of euhedral potassium feldspars and minor biotite and quartz, the latter of which are less than 10% of the rock. It occurs as small plutons in the study area, of which the Young-Davidson gold-bearing intrusion is a typical one (Fig. 3D). Syenite porphyry (or feldspar-quartz porphyritic syenite) occurs predominantly as small dikes in the eastern-middle part of the area. They show a typical porphyritic texture that is characterized by large phenocrysts (0.5–1 cm) of euhedral potassium feldspar in a medium-grained matrix of feldspar, hornblende, biotite and quartz (Fig. 3E). Minor mafic syenite intrusions occasionally occur within the coarse-grained syenite and vary in color from dark pinkish to grey (Linnen et al., 2012). Mafic syenite contains a greater amount of mafic minerals (e.g., hornblende and biotite) than syenite and syenite porphyry. Large syenite pluton is represented by the Cairo intrusion in the eastern part of the area (Fig. 2), and the Cairo and Young-Davidson intrusions have similar trace element patterns, suggesting that they belong to the same magmatic suite (Martin, 2012). The Cairo intrusion shows mostly coarse grained texture and massive structure, except the southern margin that experiences intense deformation and carbonate-chlorite-sericite alteration associated with the development of the CLLDZ (Fig. 2). Available isotopic age data show that the emplacement of the syenite intrusions largely bracket the period of 2680–2672 Ma (Ayer et al., 2005; Berger, 2006; Linnen et al., 2012), which on a regional scale is broadly contemporaneous with the deposition of the 2676–2670 Ma Timiskaming assemblage (Ayer et al., 2005).

#### 2.4. Matachewan diabase dykes

All of the Neoarchean rocks of this area are intruded and truncated extensively by Paleoproterozoic (~2470 Ma) northwest to N-S-trending Matachewan diabase dikes (Fig. 2; also see Fig. 3F; Heaman, 1997). Diabase dikes range from a few meters to 50 m in width and vertically truncate all the Neoarchean folding structures and penetrative foliations (Fig. 2). Most mafic dikes are cut by epidote-chlorite-carbonate stringers, indicating that they have been overprinted by a late hydrothermal event (Linnen et al., 2012). Late semi-brittle to brittle structures slightly reworked both the Matachewan dykes and the Neoarchean rock assemblages and may represent a Proterozoic reactivation throughout the area (Fig. 2).

### 3. Deformational history of the Matachewan area

Extensive structural investigations have focused on the middle and eastern segments of the CLLDZ (i.e., Kirkland Lake and Malartic area) and have generated numerous interpretations of the deformational history of the CLLDZ (Lovell, 1967; Sinclair, 1982; Hamilton and Hodgson, 1984; Toogood and Hodgson, 1985; Robert, 1989; Hodgson et al., 1991; Desrochers and Hubert, 1996; Wilkinson et al., 1999; Berger and Préfontaine, 2005; Ispolatov et al., 2005, 2008). However, there is a lack of detailed structural information about the western extension of the CLLDZ in the Matachewan area. Although major structures were proposed and described in the previous literature (e.g. Lovell, 1967; Powell, 1991; Berger and Préfontaine, 2005), deformational sequence and associated structures, in particular those of early generations of deformation are poorly constrained. In addition, previous studies used different nomenclatures to define the deformational sequence. For example, Robert (1989) defined D<sub>1</sub> and D<sub>2</sub> as post-Timiskaming deformations, whereas Wilkinson et al. (1999) defined D<sub>1</sub> as the pre-Timiskaming deformation and D<sub>2</sub>–D<sub>3</sub> as the post-Timiskaming deformations.

Hodgson and Hamilton (1989) defined D<sub>0</sub> as pre-Timiskaming deformation and D<sub>1</sub> as post-Timiskaming deformation. Powell and Hodgson (1992) defined the D<sub>A0</sub> to D<sub>A4</sub> as the deformational sequence that occurred in the Archean and D<sub>P1</sub> as the deformation in the Proterozoic.

In this paper, we designate D<sub>1</sub> to D<sub>4</sub> as the deformational sequence throughout the whole text. D<sub>1</sub> structures include S<sub>1</sub> (cleavage/foliation), F<sub>1</sub> (fold) and L<sub>1</sub> (lineation). D<sub>2</sub> to D<sub>4</sub> obey the same order. The reason for adopting this sequence is so that the oldest deformation event recognized in the map area is denoted as D<sub>1</sub>. It is emphasized that D<sub>1</sub> and D<sub>2</sub> in this paper are largely equivalent to the D<sub>2</sub> and D<sub>3</sub> defined by Wilkinson et al. (1999) and Berger and Préfontaine (2005). All planar structural measurements are recorded using the right-hand rule. For example, measurement 110/85 indicates a plane strikes 110° and dips to SW with a dip angle of 85°.

#### 3.1. Deformation D<sub>1</sub>: NE-SW-oriented shortening and top-to-N/NE thrusting

Based on field structural investigations and overprinting relationships, four generations of deformation (D<sub>1</sub>–D<sub>4</sub>) were identified in the Matachewan area. D<sub>1</sub> deformation is the earliest generation of deformation recognized in the area and is characterized by regional upright and tight to isoclinal folds (F<sub>1</sub>) and fold axial planes (S<sub>1</sub>). D<sub>1</sub> deformation can be subdivided into early stage D<sub>1a</sub> and late stage D<sub>1b</sub>. During the D<sub>1a</sub> deformation, both volcanic and Timiskaming metasedimentary rocks were folded and tilted to a sub-vertical orientation (Fig. 2). F<sub>1a</sub> folds are rarely preserved and are difficult to identify on meter-scale outcrops due to lack of penetrative fold axial planar cleavages. However, F<sub>1a</sub> folds can be distinguished and traced by the tightly folded and repeated compositional layering or bedding S<sub>0</sub> at certain locations in the Matachewan area. A large-scale F<sub>1a</sub> fold can be reconstructed by identifying repetition of several northwest-trending bands of older mafic volcanic rocks intercalated with the younger Timiskaming sedimentary rocks, as shown in Fig. 2. Within each band, several secondary F<sub>1a</sub> anticlinal and synclinal folds were characterized by opposite orientations of the younging indicators and sub-vertically dipping beddings (Fig. 2). Small-scale F<sub>1a</sub> folds can be identified in weakly deformed areas, on the basis of the opposite stratigraphic younging indicators (e.g., flattened pillows or graded bedding; Fig. 4A and B). Similar syn- or anticlines were also determined within the middle band of the mafic volcanic rocks (Fig. 2). Folded bedding dips steeply to the SSW and NNE, respectively (Fig. 4C). Variable orientation of the original bedding indicates a late superimposition by subsequent D<sub>1b</sub>, D<sub>2</sub> and D<sub>3</sub> (Fig. 4C).

D<sub>1b</sub> deformation was the result of a progressive NE-SW-oriented shortening and generated the dominant structures of the Matachewan area, including penetrative foliations S<sub>1b</sub>, top-to-N/NE thrust faults, and mineral stretching lineations L<sub>1b</sub>. S<sub>1b</sub> is commonly penetrative and heterogeneously overprints the tilted bedding at a small angle (Fig. 4D and E). For example, in the northern band of the Timiskaming sedimentary rocks, S<sub>1b</sub> penetrative foliation truncates the sub-vertical bedding and dips sub-vertically to SW (Fig. 4D). Regionally the S<sub>1b</sub> foliation shows preferred NW-SE-trending in orientation with variable strikes from mostly northeast to east (Fig. 4F), which is most likely the consequence of superimposition by subsequent D<sub>2</sub> and D<sub>3</sub> deformations.

Developing progressively upon the fabrics of the earlier D<sub>1a</sub> (tilting of Tisdale and Timiskaming assemblages), the D<sub>1b</sub> deformation produces L<sub>1b</sub> mineral/stretching lineations on the penetrative S<sub>1b</sub> foliations, and top-to-N/NE reverse faults are developed at the late of D<sub>1b</sub> as a result of strain accumulation. In the mafic volcanic rocks, L<sub>1b</sub> lineation is defined by oriented chlorite and sericite aggregates, whereas in the Timiskaming metasedimentary rocks

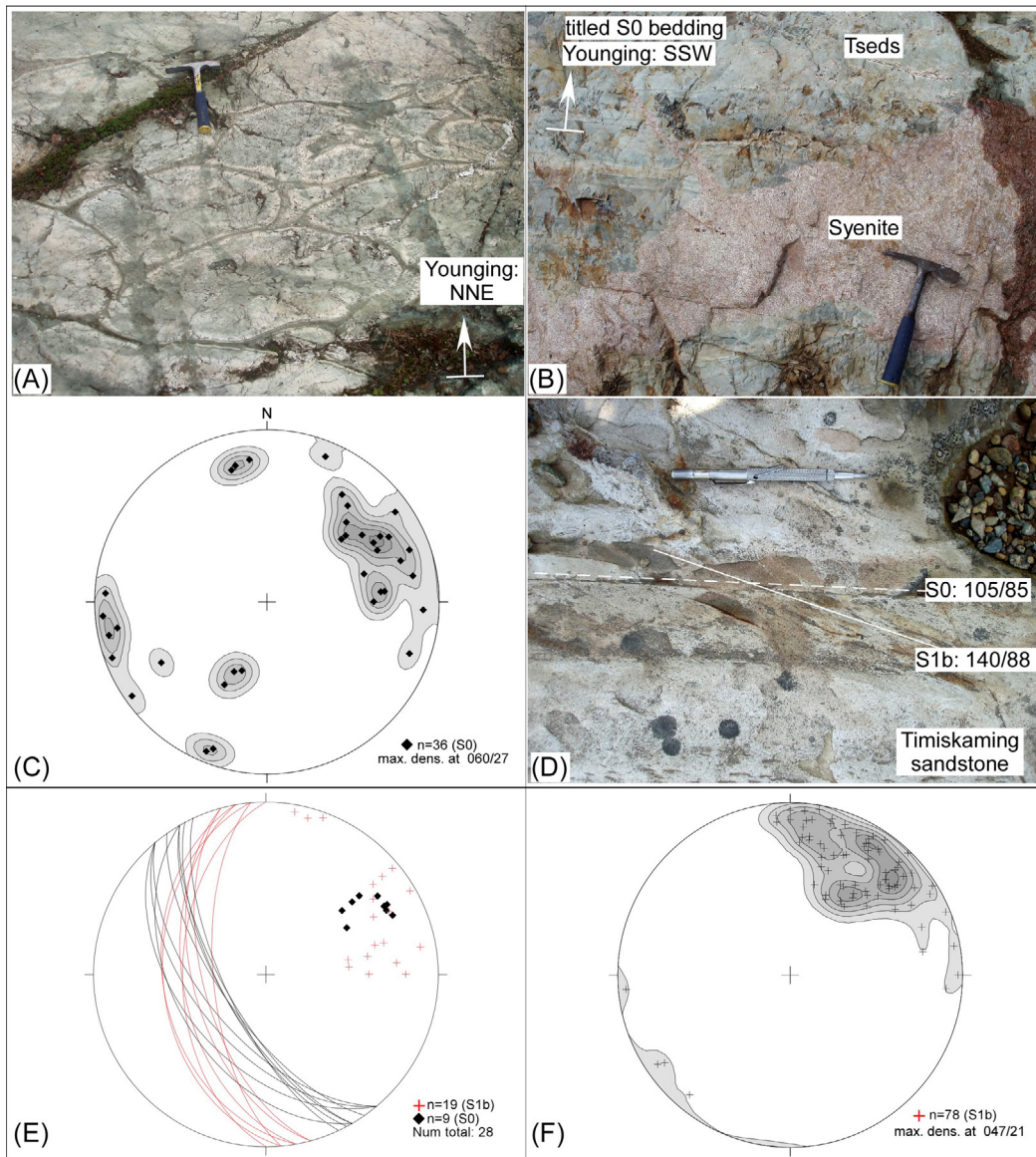


**Fig. 4.** Regional  $D_{1a}$ – $D_{1b}$  deformational fabrics. All photos show sub-horizontal surfaces. All planar structural measurements are recorded using the right-hand rule. For example in Fig. 4D, measurement 140/88 indicates a plane strikes  $140^\circ$  and dips to SW with a dip angle of  $88^\circ$ . (A) Weakly deformed pillows in the middle band of the mafic volcanic rocks, showing younging direction to the NNE. (B) Graded bedding in a Timiskaming sedimentary rock (Tseds, sandstone), showing younging direction to the SSW. Syenite intrudes into the pre-tilted sedimentary rocks. (C) Equal-angle lower-hemisphere projection of poles to  $S_0$  bedding. Variation of  $S_0$  is the result of  $D_{1a}$ , as well as  $D_{1b}$ ,  $D_2$  and  $D_3$ . (D) Penetrative  $S_{1b}$  foliation overprinting the  $S_0$  bedding at a small angle. (E) Equal-angle lower-hemisphere projection showing the small angle overprinting relationship between  $S_0$  and  $S_{1b}$ , which is consistent with field observation (Fig. 4D). (F) Equal-angle lower-hemisphere projection of regional penetrative  $S_{1b}$  foliation. Variation of  $S_{1b}$  is a result of late superimposition by  $D_2$  and  $D_3$ .

$L_1$  is defined by elongated clasts and stretched pebbles (Fig. 5). The best exposure of  $L_{1b}$  lineation is located at the edge of the Open pit 4 of the Young-Davidson mine site (Fig. 5A), in which the Timiskaming metasedimentary rocks are tectonically in contact with mafic volcanic rocks. The  $S_{1b}$  foliation observed on this outcrop dips to SW at moderate to steep angles (Fig. 5B). Measured on  $S_{1b}$ ,  $L_{1b}$  lineations are characterized by stretched pebbles and chlorite aggregates that are heterogeneously deformed to be different shapes on different planes (Fig. 5C). On YZ plane, pebbles keep mostly the original round shape and are rarely deformed or stretched. On XY plane, pebbles have been stretched to be ellipses, indicating a vertical stretching during  $D_{1b}$ . On XZ plane, pebbles are intensely flattened and stretched and are incorporated into the newly developed  $S_{1b}$ .  $L_{1b}$  lineations plunge to the SW at moderate to high angles, indicating a dominant sub-vertical stretching deformation during  $D_{1b}$ .  $D_{1b}$  also generates a series of top-to-N/NE

thrust faults throughout the highly deformed domains. Kinematic indicators such as oblique fabrics within the  $S_{1b}$  foliations indicate apparently a top-to-N/NE sense of shear and thrust (Fig. 5D). Inside the Young-Davidson gold-bearing syenite intrusive body, displacement of pre- $D_{1b}$  ankerite-quartz-pyrite veins by  $D_{1b}$  thrust faults also indicate a top-to-NE sense of thrust (see below).

Regionally, syenite intrusions intruded into both of the steeply tilted mafic volcanic and Timiskaming sedimentary rocks that were formed during  $D_{1a}$  (Fig. 4B). As shown in Fig. 4B, the xenolith is Timiskaming sedimentary rock, of which the bedding has been tilted to be sub-vertical in orientation. Many of these xenoliths are preserved in the Cairo stock (Fig. 2), which is a large intrusion and is unlikely tilted by the  $D_{1a}$  isoclinal folds. Meanwhile syenite intrusions are pervasively overprinted by  $S_{1b}$  penetrative foliations (Fig. 6A). Emplacement of the syenite is coeval with the late  $D_{1a}$  and predates the  $D_{1b}$ . This suggests that the Matachewan syenites

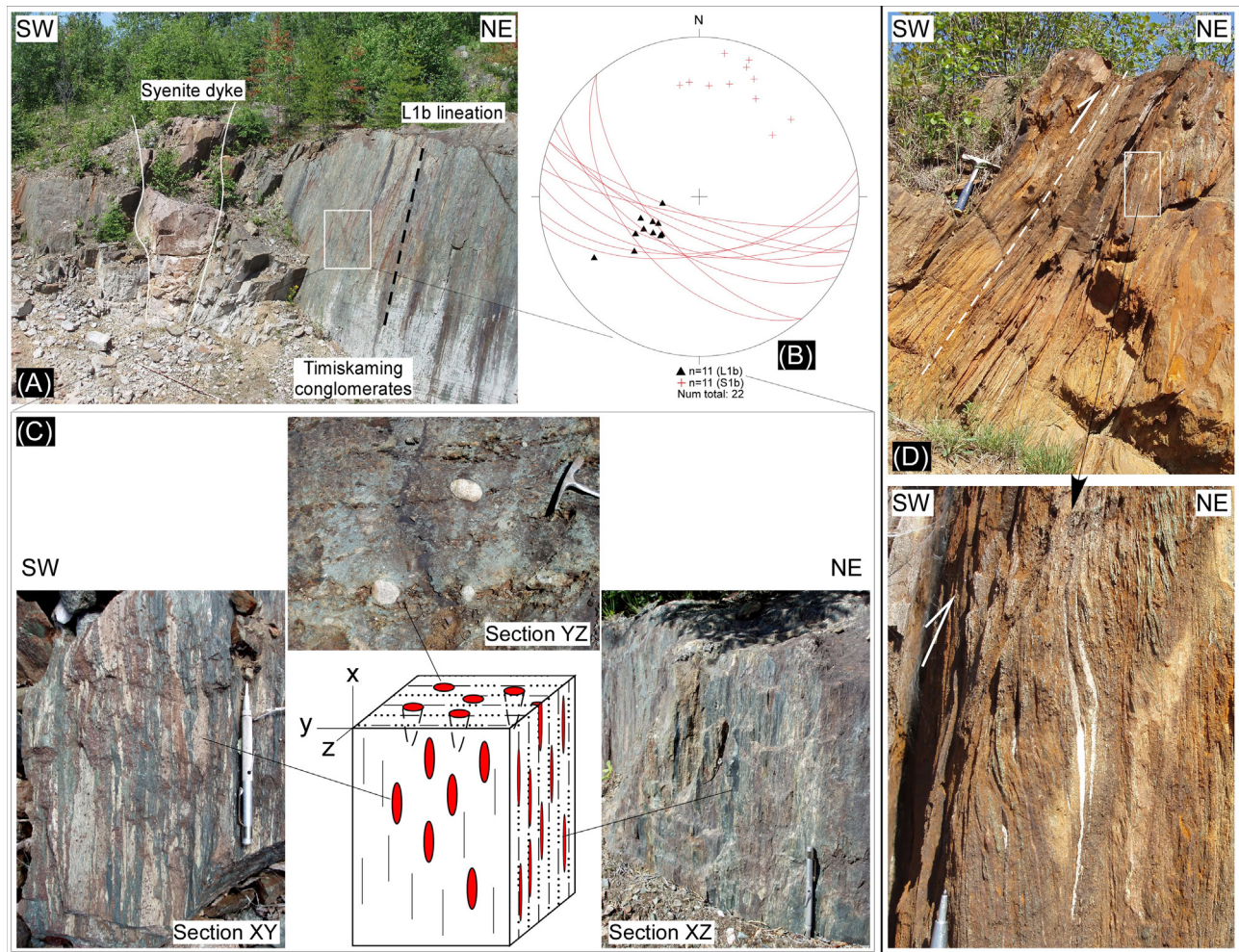


**Fig. 5.**  $D_{1b}$  fabrics in Timiskaming conglomerate, indicating a dominant top-to-N or NNE shearing during  $D_{1b}$ . (A) Highly deformed Timiskaming conglomerate.  $L_{1b}$  lineation is defined by highly stretched pebbles. (B) Equal-angle lower-hemisphere projection showing poles to  $S_{1b}$  and  $L_{1b}$ . (C) Block diagram and photos showing contrasting geometry of deformed pebbles on three principal planes, indicating strong vertical stretching. On the  $YZ$  plane, the aspect ratios (ratio of long/short axis) of the pebbles are very low, on the  $XY$  plane, the ratio is high, and on the  $XZ$  plane, the ratio is very high and it is hard to distinguish the deformed pebbles from the matrix. (D) Asymmetric fabrics showing consistently top-to-NE shearing.

are syn-tectonic intrusions.  $D_{1a}$  upright folding, emplacement of the syenites, and the development of the regional penetrative  $S_{1b}$  foliations are broadly synchronous.

Horizontal shortening during the  $D_1$  deformation led to the crustal thickening and subsequent sub-greenschist to greenschist facies metamorphism. The development of regional greenschist facies metamorphism is dominated by the  $D_{1b}$  fabrics.  $S_{1b}$  penetrative foliations in the mafic volcanic rocks are characterized by extensive chlorite–carbonate–fuchsite alteration.  $S_{1b}$  foliations within syenites have mineral assemblage of chlorite + carbonate + sericite + feldspar + pyrite  $\pm$  biotite (Fig. 6A). This implies that the metamorphism, metasomatism and alteration may have occurred synchronously due to the existence of hydrothermal fluid.

### 3.2. Deformation $D_2$ : top-to-NW oblique thrusting and dextral strike-slip shearing

$D_2$  deformation occurred under a NW–SE-oriented shortening and is characterized by top-to-NW oblique thrusting and dextral strike-slip shearing. The main structure of CLLDZ is largely associated with  $D_2$ . Associated with the  $D_2$  deformation are the development of variable scales of  $F_2$  folds,  $S_2$  crenulation cleavages to penetrative foliations, and  $L_2$  intersection lineations

and mineral lineations.  $D_2$  deformation can be subdivided into early- $D_2$  and late- $D_2$ . Early- $D_2$  is responsible for the development of  $F_2$  folds,  $F_2$  axial planar cleavages  $S_2$ , and lineations  $L_2$ ; whereas late- $D_2$  resulted in the development of  $S_2$ – $C_2$  composite fabrics corresponding to a regional dextral strike-slip shearing deformation.

During the early  $D_2$ , regional  $S_{1b}$  foliations were folded into open to tight  $F_2$  asymmetric folds that plunge moderately to steeply to SW (Fig. 6B and C), except the locus of high strain zone in which they are intensely folded into isoclinal folds (see below). Both the earlier  $S_0$  bedding and  $S_{1b}$  foliation were reworked by  $F_2$  folds (Fig. 6D). In the weakly deformed area, a successive overprinting relationship between  $S_0/S_{1b}$  composite fabrics and  $F_2$  can be observed in the Timiskaming metasedimentary rocks. Although  $S_0/S_{1b}$  retains the low-angle overprinting relationship, both of them have been refolded to variable orientations by  $F_2$  folds (Fig. 6D). Most  $F_2$  folds are asymmetric “Z”-type folds, which were previously considered to represent  $D_2$  dextral shear deformation (Berger and Préfontaine, 2005; Berger, 2006). However, our recent mapping results show that the ‘Z’-type  $F_2$  asymmetric folds most possibly represent one deformed limb of a larger-scale  $F_2$  fold, while the other limb is characterized by ‘S’-type asymmetric folds (Linnen et al., 2012).  $F_2$  folds are therefore interpreted to have resulted from a NW–SE-oriented shortening during the early  $D_2$  deformation.

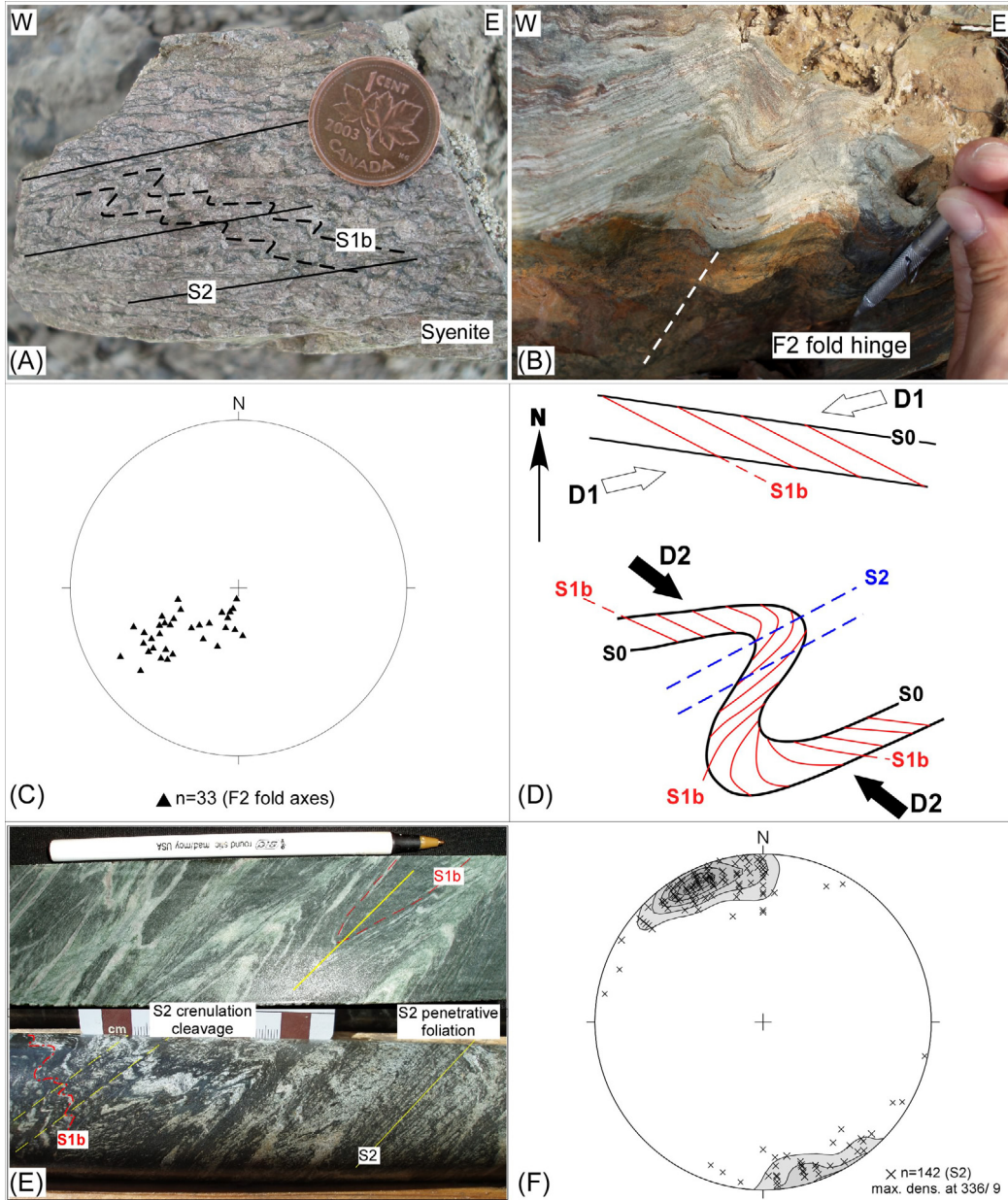


**Fig. 6.** Regional D<sub>2</sub> fabrics. (A) S<sub>1b</sub>/S<sub>2</sub> composite fabrics in a syenite, indicating that it experienced both D<sub>1b</sub> and D<sub>2</sub> deformations. (B) F<sub>2</sub> asymmetric folds with steeply SW-plunging fold hinge lines. (C) Equal-angle lower-hemisphere projection showing that the F<sub>2</sub> folds are moderate to steep S-SW plunging, which is consistent with field observation (Fig. 6B). (D) Sketch showing the S<sub>0</sub>/S<sub>1b</sub> composite fabrics folded by F<sub>2</sub> open fold. (E) S<sub>1b</sub>/S<sub>2</sub> transposition observed in drill core. S<sub>1b</sub> foliation is folded and transposed to S<sub>2</sub>. (F) Stereonet plot of poles to regional S<sub>2</sub> foliations. Variation of S<sub>2</sub> indicates a late superimposition by D<sub>3</sub>.

F<sub>2</sub> axial planes (S<sub>2</sub>) display as the crenulation cleavages in the most locations. Close to and within the high strain zone (e.g. CLLDZ), progressive shortening and incremental strain progressively transpose the S<sub>2</sub> crenulation cleavage into penetrative S<sub>2</sub> foliation (Fig. 6E). S<sub>2</sub> dips steeply to the NNW and partly to the SSE; the slight variations are due to late D<sub>3</sub> superimposition (Fig. 6F). Two types of lineations are associated with the development of D<sub>2</sub>. A L<sub>2</sub> intersection lineation is extensively developed on the S<sub>2</sub>/S<sub>1b</sub> composite fabrics (Fig. 7A), consistently with the orientation of F<sub>2</sub> fold axis that plunge to the SW at a high angle. An L<sub>2</sub> mineral lineation is characterized by chlorite + sericite aggregates that developed on the penetrative S<sub>2</sub> foliations (Fig. 7B). In the middle of the high strain zone, mineral lineations indicate a sub-vertical shearing (Fig. 7C). Plots of overall mineral lineations throughout the deformation zone (e.g. CLLDZ) show that the plunging of L<sub>2</sub>

mineral lineations varies from moderately WSW to steeply ENE (Fig. 7D). This trend is consistent with the field kinematic indicators that D<sub>2</sub> experienced under a NW-SE-oriented shortening and an oblique slip thrusting and an ENE trending dextral shearing, which were dominantly localized in the middle part of the CLLDZ.

Successive shortening led to a subsequent nearly E-W-trending dextral strike-slip shearing, which characterizes the late D<sub>2</sub> deformation. These late D<sub>2</sub> ductile shear zones are dominantly developed along the contacts between different lithological units (Fig. 2). As shown in an outcrop-scale detailed map (Fig. 8A), the earlier S<sub>2</sub> spaced crenulation cleavage is progressively compressed and transposed into penetrative foliation (Fig. 8B), and is finally incorporated by the newly formed shear planes (Fig. 8C). Asymmetry between S<sub>2</sub> and shear planes indicates a dextral sense of

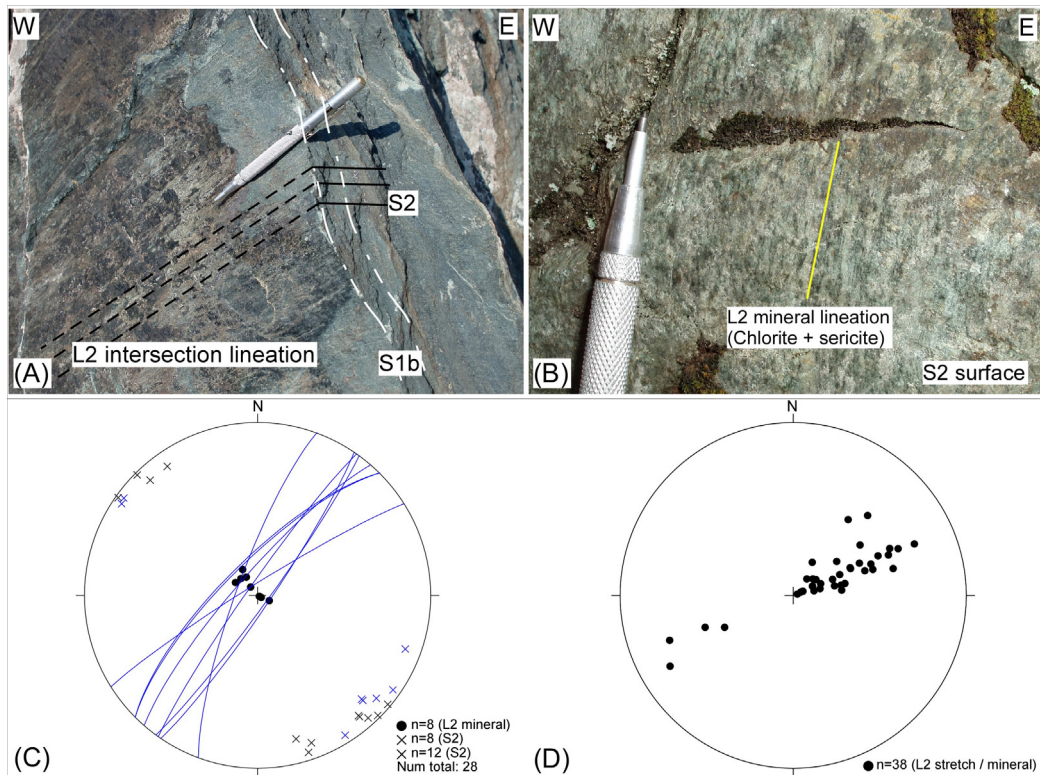


**Fig. 7.** L<sub>2</sub> lineations. (A) L<sub>2</sub> intersection lineation in the mafic volcanic rocks plunges to the SW, consistent with the orientation of F<sub>2</sub> fold axis. (B) Steeply plunging L<sub>2</sub> mineral lineations are composed of chlorite + sericite, indicating a greenschist facies of metamorphism during D<sub>2</sub>. (C) S<sub>2</sub>-L<sub>2</sub> fabrics showing steeply plunging L<sub>2</sub> mineral lineations, consistent with the field observation (Fig. 7B). (D) Stereonet plot showing moderately to steeply plunging L<sub>2</sub> stretching lineations.

shear (Fig. 8C). Outside the shear zone rocks are weakly deformed and the original depositional structures are well preserved (Fig. 8D).

Similar deformational episode and associated structures were also well reported in the middle and eastern segments of the CLLDZ, which are summarized in Table 1 (Robert, 1989; Hodgson et al., 1991; Wilkinson et al., 1999; Ispolatov et al., 2008; Lafrance, 2009). Overall the D<sub>2</sub> fabric of the Matachewan area shows similar geometry and an intimate relationship with that of the CLLDZ (Table 1). The metamorphism grade during D<sub>2</sub> is estimated to be under greenschist facies, which is represented by mineral assemblage of chlorite + sericite + carbonate ± epidote that forms the S<sub>2</sub> penetrative foliation.

### 3.3. Deformation D<sub>3</sub>: semi-brittle deflection of the CLLDZ

D<sub>3</sub> deformation developed under a NE-SW shortening, which produced numerous "S"-type F<sub>3</sub> open folds and associated fold axial plane S<sub>3</sub>. F<sub>3</sub> are largely asymmetric and open folds, which refolded the limbs of earlier F<sub>2</sub> isoclinal fold into a composite F<sub>2</sub>-F<sub>3</sub> interference pattern (Fig. 9A and B). Traces of F<sub>3</sub> fold axes can locally be measured on the folded penetrative S<sub>2</sub> foliations. F<sub>3</sub> fold plunges steeply to NE and S<sub>3</sub> planes dip to the NE at a high angle (Fig. 9B and C). S<sub>3</sub> planes are semi-brittle to brittle cleavages without a new mineral assemblage (Fig. 9D), indicating that the pressure-temperature (P-T) condition of D<sub>3</sub> is much lower than that of the earlier D<sub>1</sub> and D<sub>2</sub> deformations. No specific age constraining the D<sub>3</sub> deformation has been obtained because of lacking the suitable minerals for isotopic age dating. However such D<sub>3</sub> fabrics have been truncated and reworked by regional Neoarchean NE/N-trending faults (e.g. Holmes lake fault in the Holmes Township), suggesting a Neoarchean age (e.g. Powell and Hodgson, 1992).

### 3.4. Deformation D<sub>4</sub>: brittle faulting in Proterozoic

D<sub>4</sub> deformation is characterized by variable scales of brittle faults, most of which truncate and displace the D<sub>1</sub> to D<sub>3</sub> fabrics of this area. The large-scale brittle faults are regional-scale N-S-trending Mistinikon Lake fault and Montreal River fault, which apparently displace the Neoarchean rocks along a north-south orientation (Fig. 2). The meso-scale brittle faults are SE-trending and SW-dipping faults that transverse the southern area. A sharp boundary between the Gowganda Formation and the Tisdale mafic volcanic rocks to the SW suggests a possible fault-controlled Proterozoic deposition (Fig. 2). The small-scale faults are outcrop-scale NE-trending faults, most of which show obviously left-lateral displacement (Fig. 9E). Locally the mafic dyke was slightly folded, indicating an approximately NE-SW shortening event after its emplacement (Fig. 9F). Similar gentle folds were well preserved in the adjacent Gowganda Formation of the Matachewan area and therefore could represent a weak Proterozoic shortening event (Powell and Hodgson, 1992). This Proterozoic shortening may also cause a reactivation of faults in the Archean basement and produced a series of left-lateral strike-slip faults (Fig. 9E). Although these faults show similar orientations with the major structure of the CLLDZ, their truncation and displacement of the Matachewan mafic dike suggest a Proterozoic age (Fig. 9F). Narrow zones of enriched sulfides are locally associated with these faults, indicating a possible Proterozoic hydrothermal reactivation on the Neoarchean structures within the CLLDZ (e.g. Powell and Hodgson, 1992).

## 4. Syenite-hosted veins and associated gold mineralization

Gold was first reported in the Matachewan area in 1901, and the Young-Davidson and Matachewan Consolidated mines were discovered in 1916 and 1917, respectively (Lovell, 1967;

**Table 1**  
Deformational generations and the associated structural features of the CLLDZ.

Author	This study	Hodgson et al. (1991)	Wilkinson et al. (1999)	Ispolatov et al. (2008)	Robert (1989)
Relative location of the CLLDZ	Western segment, Matachewan, Ontario	Middle segment, Larder Lake area, Ontario	Middle segment, Kirkland Lake area, Ontario	Middle segment, Kirkland Lake – Larder Lake area, Ontario	Eastern segment, Val d'Or area, Québec
Possible earlier generation	Not found	Not found	D <sub>1</sub> : nearly E-W trending upright anticlines and synclines. Only preserved within Pre-Timiskaming volcanic rocks.	D <sub>1</sub> : follow the definition by Wilkinson et al. (1999).	Not found
First (1st) generation	1. D <sub>1a</sub> : nearly NE-SW shortening. 2. F <sub>1a</sub> : NW-SE trending upright isoclinal folds without penetrative foliations. Coeval with the latest stage of the Timiskaming sedimentation and the syenite emplacement. 3. D <sub>1b</sub> : progressively NE-SW shortening. Top-to-NE reverse faults. 4. S <sub>1b</sub> : NW trending penetrative axial planar foliations.	1. D <sub>1</sub> : NNE compression, oblique sinistral movement on LLDZ. Top-to-NE thrust faults. 2. S <sub>1</sub> : WNW trending axial planar foliation to WNW trending upright, tight to isoclinal folds. 3. S <sub>1</sub> is variably overprinted by S <sub>2</sub> .	1. D <sub>2</sub> : nearly N-S shortening; E-W trending segments of the CLLDZ accumulate bulk coaxial compression, NE and SE-trending segments experience dextral and sinistral transpressional deformation, respectively. 2. S <sub>2</sub> parallel to the CLLDZ: strike varies from ENE (NE trending segment) gradually to nearly E-W (E-W trending segment) and ESE (SE trending segment).	1. D <sub>2</sub> : nearly N-S shortening; mostly penetrative WNW-striking steeply dipping foliation. 2. Oblique Reverse-dextral shearing deformation (south side over north). 3. D <sub>2</sub> structures largely define the CLLDZ.	1. D <sub>1</sub> : nearly N-S shortening, sub-vertical shearing, local dip-slip movements, synchronous dextral shearing. S <sub>1</sub> : WNW to nearly E-W trending. S <sub>1</sub> obliquely overprints the CLLDZ lithological contact.
Second (2nd) generation	1. D <sub>2</sub> : NW-SE shortening, oblique dextral shearing. 2. S <sub>2</sub> : NE to nearly E-W trending steeply crenulation cleavage to penetrative foliation. 3. Late D <sub>2</sub> is a series of nearly E-W trending oblique-slip shear zones which are parallel to the CLLDZ.	1. D <sub>2</sub> : NW-SE compression, oblique dextral movement on CLLDZ (south side up). 2. S <sub>2</sub> : E-W to NE-trending steeply dipping crenulation cleavage. Largely parallel to the CLLDZ.	1. D <sub>3</sub> : NW-SE shortening, dextral reactivation of SE and EW-trending segments of the CLLDZ. 2. S <sub>3</sub> : sub-vertical NE-striking crenulation axial planar cleavage to asymmetric folds.	1. D <sub>3</sub> : E-W shortening. 2. S <sub>3</sub> : N-S trending crenulation cleavage. Less penetrative. Such N-S trending cleavages are not commonly distributed throughout the CLLDZ.	1. D <sub>2</sub> : dominantly transcurrent dextral shear accompanied with shortening. S <sub>2</sub> : NE-SW to E-W trending spaced axial planar crenulation cleavage to a series of 'Z'-type sub-upright asymmetric folds.
Third (3rd) generation	1. D <sub>3</sub> : NE-SW shortening. Semi-brittle deformation. S <sub>3</sub> : NW trending sub-vertical axial planar cleavage along the NW trending 'S'-type open to close folds	Not reported	Not reported	1. D <sub>4</sub> : NW-SE shortening. Differentiated crenulation cleavage. S <sub>4</sub> : NE trending cleavage to 'Z'-type asymmetric folds. Show similar orientation with S <sub>2</sub> .	Not reported

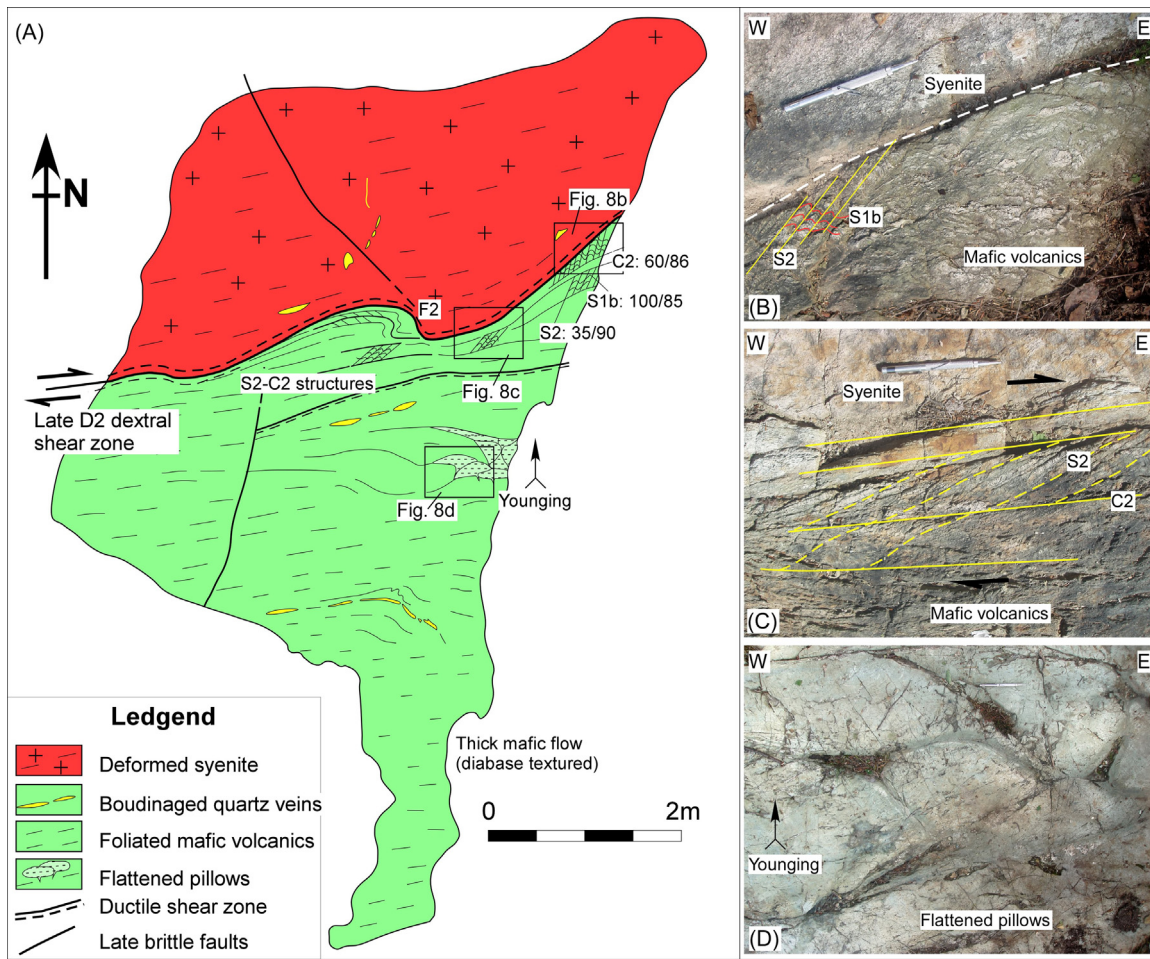


**Fig. 8.** Detailed outcrop-scale structural map showing intrusive and deformational overprinting relationships. Oka Property, 4 km northeast to the Young-Davidson Gold Deposit. (A) Syenite intrudes into mafic volcanic rocks, both of which experienced polyphase deformations. (B)  $S_{1b}$  foliations are penetrative and strike NW-SE. Subsequent  $F_2$  folds crenulated  $S_{1b}$  to form  $S_2$  penetrative cleavage. (C) Progressive deformation incorporated  $S_2$  into the subsequent E-W-oriented dextral shearing deformation along a narrow shear zone (late  $D_2$  dextral shear zone as described in the text). (D) Outside the narrow shear zone, mafic volcanic rocks are only weakly deformed and pillows can be well preserved.

(Sinclair, 1982). Mineralization in the two mines is spatially continuous, and is considered to be one deposit, the Young-Davidson deposit. The deposit is located 1 km west of the town of Matanechewan (Fig. 2).

Most of the mineralization zone is contained within the syenite intrusion and pinches out in the host mafic volcanic and Timiskaming metasedimentary rocks (Fig. 10). Mineralization is dominantly associated with multiple generations of veins in the syenite intrusion, and to a much lesser extent in the metavolcanic and metasedimentary wall rocks, although mineralization is also disseminated in the syenite (Martin, 2012). This work focuses on the vein systems within the syenite, to evaluate the structural controls on their formation, orientation, alteration and associated mineralization. Detailed structural and petrological mapping are carried out on both surface of the Young-Davidson mine and in underground drifts. In particular, a detailed underground mapping along the No. 9 ore crosscut was carried out, to thoroughly elucidate the overprinting relationships between veining and regional structures (see Inline Supplementary Fig. 1). The No. 9 ore crosscut trends N-S, is located 200 m beneath surface and crosscuts the lithological boundary between the syenite and the hosting Timiskaming metasedimentary rocks and the major mineralization zone (Fig. 10). A detailed map of both of the east and the west walls, showing lithologies, veining, gold assay results and regional structures is shown as Inline Supplementary Fig. 1 and a representative part of the map is shown as Fig. 11. Overall, four distinct stages of veining

( $V_1$ - $V_4$ ) were identified throughout the syenite intrusion, based on their crosscutting relationships and mineralogy.

Inline Supplementary Fig. S1 can be found online at <http://dx.doi.org/10.1016/j.precamres.2014.04.007>.

#### 4.1. $V_1$ vein

$V_1$  is the earliest vein set that cuts the Young-Davidson syenite intrusion (shown in grey in Fig. 11). It is characterized by folded and boudinaged ankerite (iron carbonate)-quartz-pyrite veins that dip to the south at moderate to high angles (Fig. 12A and B).  $V_1$  veins vary in thickness from several centimeters to 20 cm and are strongly deformed (Fig. 12A). Locally  $V_1$  veins have been intensely folded and crenulated, and a new axial planar foliation is developed, defined by aggregates of chlorite + sericite + pyrite (Fig. 12C). The new foliation correlates with the regional  $S_{1b}$  foliations described above (Fig. 5D). At some locations, the  $V_1$  veins are boudinaged and displaced by a series of top-to-N reverse faults (Fig. 12D) that are correlated with the regional  $D_{1b}$  reverse faults, described above (Fig. 5D). These structural relationships indicate that the  $V_1$  veins predate the  $D_{1b}$  deformation.

Petrological analysis indicates that  $V_1$  veins are composed of 70–80% ankerite, 10–15% quartz, and minor amounts of pyrite and potassium feldspar (Linnen et al., 2012). Pyrite associated with the  $V_1$  veins have corroded and fractured grain boundaries and detailed petrographic study has identified minor gold along the fractures

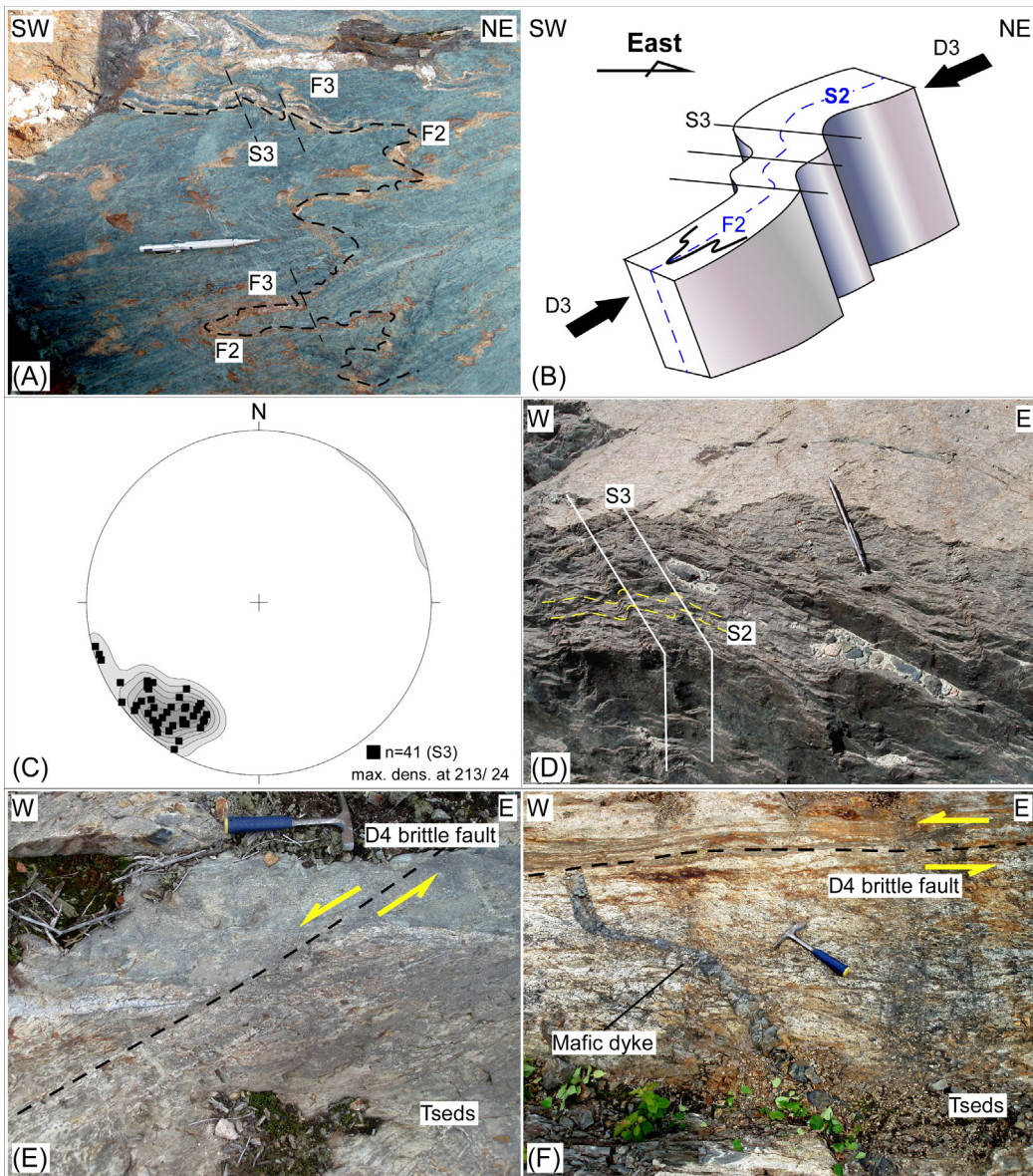


**Fig. 9.** Regional D<sub>3</sub>–D<sub>4</sub> structures. (A) F<sub>2</sub> isoclinal folds refolded by F<sub>3</sub> folds. Note that the 'S'-type F<sub>3</sub> folds are developed on the F<sub>2</sub> fold limbs. (B) Block diagram showing the overprinting relationships between D<sub>2</sub> and D<sub>3</sub>. D<sub>3</sub> is developed under a NE-SW-oriented shortening. (C) Stereonet plots of poles to S<sub>3</sub> cleavages. (D) S<sub>3</sub> semi-brittle to brittle cleavages characterize axial planar to F<sub>3</sub> folds, overprinting earlier D<sub>2</sub> fabrics. (E) A D<sub>4</sub> brittle fault in Timiskaming sedimentary rocks. (F) A D<sub>4</sub> sinistral brittle fault offsetting a Paleoproterozoic mafic dyke, indicative of a Proterozoic brittle deformational event.

of or within the pyrites (Martin, 2012). However, V<sub>1</sub> veins have been pervasively overprinted by the subsequent V<sub>2</sub> quartz–pyrite veinlets which are enriched by significant amounts of sulphide (see below). Whether the gold mineralization is intimately associated with V<sub>1</sub> veins remains uncertain. However, petrologic studies have revealed that some V<sub>1</sub> veins are surrounded by red pinkish potassium-hematite halo, indicating that a pervasive potassium-hematite alteration may have occurred after V<sub>1</sub> (Linnen et al., 2012).

#### 4.2. V<sub>2</sub> vein

The second generation veins (V<sub>2</sub>) are abundant slightly folded quartz–pyrite veinlets that crosscut earlier V<sub>1</sub> veins at high angles (shown in yellow in Fig. 11). V<sub>2</sub> veins are narrow and short veinlets, usually 2–10 cm in length and a few millimeters in width (Fig. 13A). In contrast to V<sub>1</sub>, V<sub>2</sub> veins dip to the N/NE at shallow to moderate angles (Fig. 13B). They contain significantly more pyrite than V<sub>1</sub>. As shown in Fig. 12A, wherever pyrites-enriched V<sub>2</sub> veinlets develop

and crosscut V<sub>1</sub> veins, V<sub>1</sub> veins appear to contain large amounts of pyrite aggregates, indicating that V<sub>2</sub> is a distinct sulphide-rich hydrothermal veining event that overprinted V<sub>1</sub>. Locally en echelon veins of V<sub>2</sub> are developed in relatively homogeneous part of the syenite intrusion. Detailed mapping shows that V<sub>2</sub> veinlets are truncated by the D<sub>1b</sub> faults (Inline Supplementary Fig. 1), indicating that they formed before or early during D<sub>1b</sub>. In addition, the opening vector of V<sub>2</sub> en echelon veins is consistent with a NE-SW-oriented shortening and a top-to-NE shearing that characterizes the regional D<sub>1b</sub> deformation (Fig. 13A). Therefore, the development of the V<sub>2</sub> veins most probably occurred at the early stages of the D<sub>1b</sub> deformation, after formation of V<sub>1</sub> veins but before the commencement of subsequent D<sub>1b</sub> faulting. This interpretation is consistent with the observation that the V<sub>2</sub> en echelon veins are sub-perpendicular to the regional L<sub>1b</sub> lineations (Figs. 5B and 13B).

Petrological study reveals that V<sub>2</sub> is composed of variable amounts of quartz and pyrite (locally up to 90% quartz or 90% pyrite)

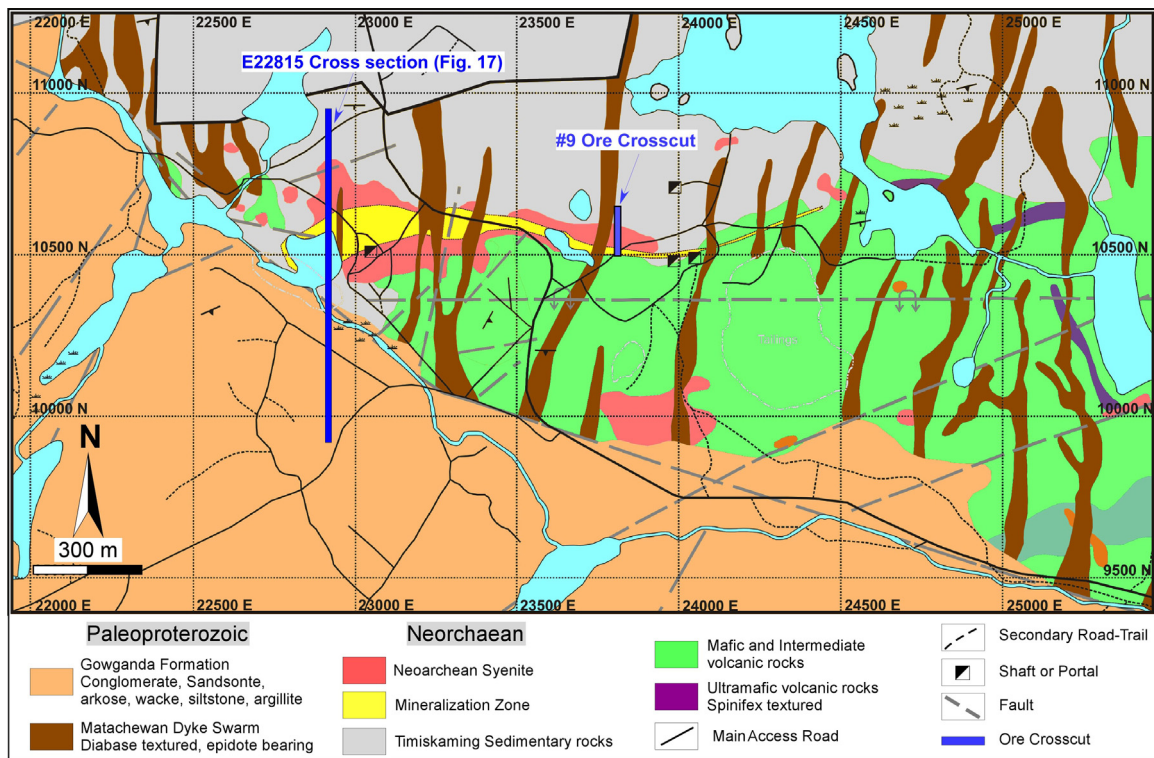


**Fig. 10.** Mine-scale geological map of the Young-Davidson gold deposit showing the distribution of major Archean rock types (modified after Lucas, 2007; unpublished data). Locations of historic and current shafts are shown and labeled. Mineralization zone is highlighted as yellow and transverses the main syenite intrusive body and pinches out in the mafic volcanic rocks to the east. The location of the No. 9 ore crosscut and E22815 cross section are projected to the surface.

with accessory carbonate, chlorite, and rutile (Linnen et al., 2012). Petrographic analysis shows that gold is present as inclusions and more commonly along fractures and cracks in the pyrite aggregates (Fig. 13C). Visible native gold (VG) is present within V<sub>2</sub> veinlets (Fig. 13D). Pyrite associated with V<sub>2</sub> are normally corroded and sub-euhedral, with abundant hematite and magnetite inclusions (Martin, 2012).

#### 4.3. V<sub>3</sub> vein

The third generations of veins (V<sub>3</sub>) are en echelon quartz–pyrite–carbonate veins (shown in blue in Figs. 11 and 14A

and B). V<sub>3</sub> veins range from 1 cm to 10 cm in width and from 20 cm to several meters in length (Inline Supplementary Fig. 1). V<sub>3</sub> en echelon veins show asymmetric sigmoidal vein arrays that split and crosscut V<sub>2</sub> veins (Fig. 14A). However, some V<sub>3</sub> veins are crosscut and overprinted locally by a series of thin planar carbonate-quartz V<sub>4</sub> veins (Fig. 14B). V<sub>3</sub> en echelon veins occur throughout the Young-Davidson syenite intrusion.

Like V<sub>2</sub>, V<sub>3</sub> veins dip to the NE but at moderate to shallower angles (Fig. 14C). The geometry and orientation of the V<sub>3</sub> veins are also consistent with a NE-SW-oriented shortening and top-to-NE shearing that is consistent with the D<sub>1b</sub> deformation. In contrast with the V<sub>2</sub> veins, some V<sub>3</sub> veins are truncated by the D<sub>1b</sub>

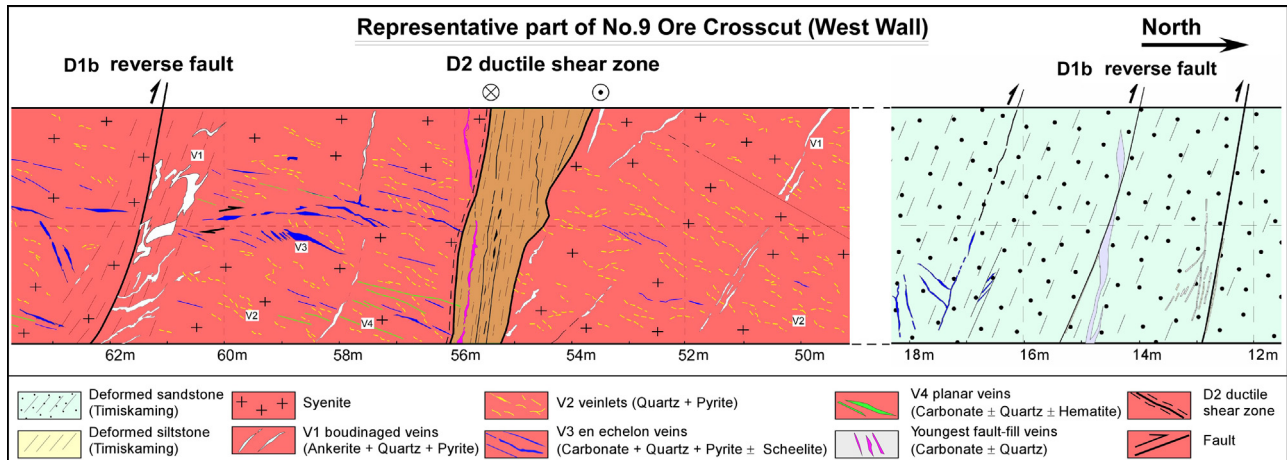


**Fig. 11.** Representative part of a cross section of the No. 9 ore crosscut (West Wall) showing the major structures and types of veining. Refer to [Inline Supplementary Fig. 1](#) for the full cross section and detailed descriptions in text. (For interpretation of the references to color in this figure legend, the reader is referred to the web version of the article.)

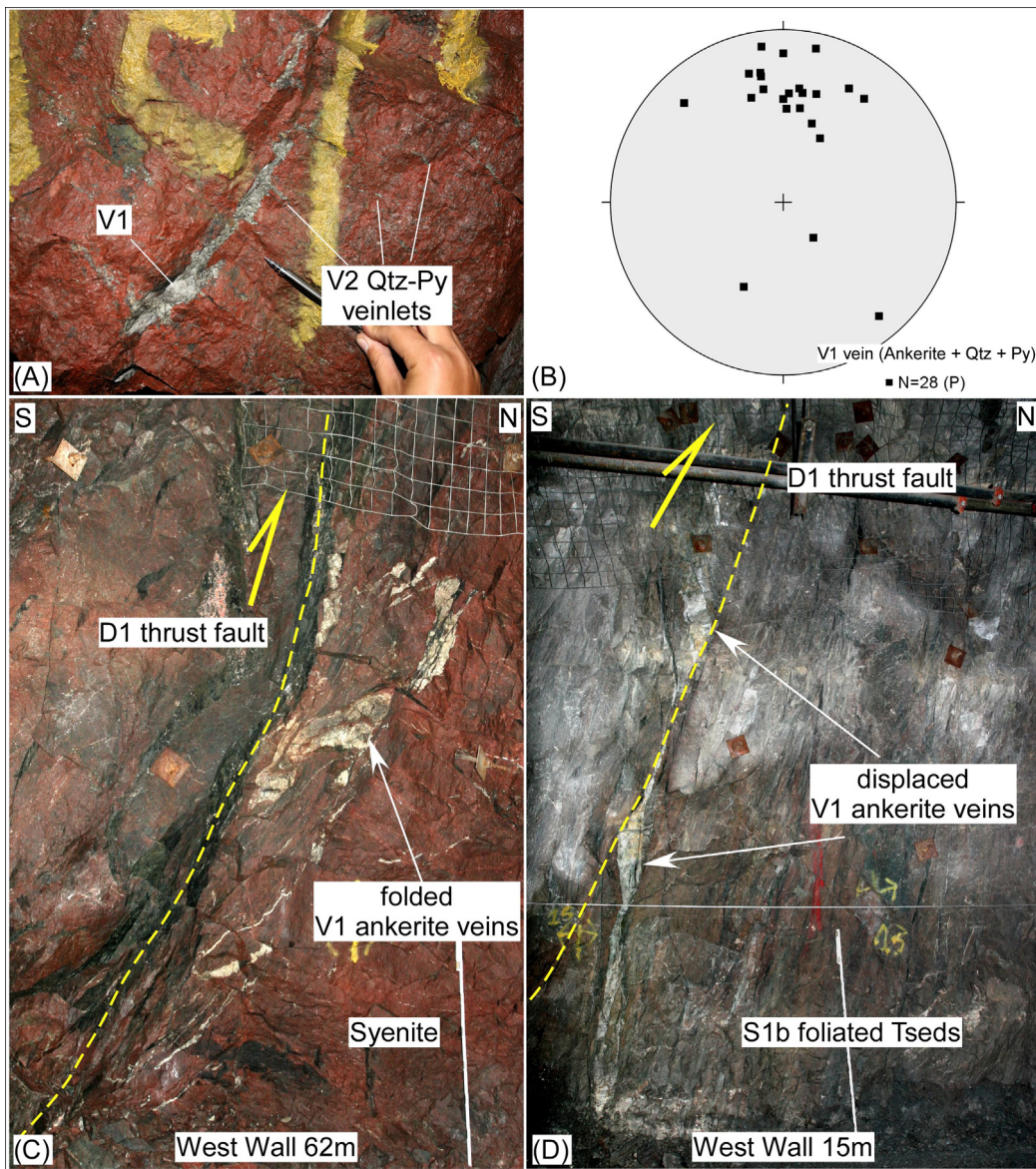


**Fig. 12.**  $V_1$  veins. Locations (e.g. West Wall 62 m) are labeled on some photos. (A) Boudinaged steeply S-dipping  $V_1$  Ank + Qtz + Py veins overprinted and crosscut by NE-dipping  $V_2$  Qtz + Py veinlets. (B) Equal-angle lower-hemisphere projection of poles to  $V_1$  veins. (C)  $V_1$  Ank + Qtz + Py veins folded and boudinaged and reworked by the  $D_{1b}$  top-to-N thrust fault. (D)  $V_1$  veins displaced by  $D_{1b}$  fault with a top-to-N sense of shear. Abbreviations: Ank—Ankerite, Cab—Carbonate, Cpy—Chalcopyrite, Hem—Hematite, Sch—Scheelite, Py—Pyrite, Qtz—Quartz, Tseds—Timiskaming sedimentary rocks.

faults, whereas some other  $V_3$  veins cut them. Such a mutual cross-cutting relationship indicates that  $V_3$  veins are syn-tectonic veins that developed synchronously with the  $D_{1b}$  top-to-NE shearing or thrusting deformation.

$V_3$  is composed of quartz and carbonate with accessory pyrite, chalcopyrite, minor scheelite, potassium feldspar and chlorite (Linnen et al., 2012). Petrographic study shows that pyrites in  $V_3$  are mostly euhedral, clean and less corroded, containing much less mineral inclusions than  $V_1$  and  $V_2$  (Martin, 2012). Inclusions in the  $V_3$  pyrite are typically galena, chalcopyrite and minor rutile, in contrast to the hematite–magnetite–rutile rich inclusions in  $V_2$ . Gold associated with  $V_3$  usually occurs along fractures of the euhedral pyrites. Results from core logging also show that  $V_3$  veins contain scheelite and occurrences of visible native gold along the quartz–carbonate vein boundaries (Fig. 14D). Red pinkish Kfeldspar-hematite halos are well developed around  $V_3$  veins (Fig. 14D). Mineralized  $V_3$  en echelon veins are pervasively folded and crenulated by the  $F_2$  folds,

indicating that their formation predates the regional  $D_2$  deformation (Fig. 14E).

#### 4.4. Pre- $V_4$ E-W-trending $D_2$ ductile shear zone

Based on the crosscutting relationship, the earlier  $V_2$  and  $V_3$  veins have been truncated by a series of nearly E-W-trending ductile shear zones which are crosscut by the subsequent  $V_4$  veins (Inline Supplementary Fig. 1). These shear zones are generally narrow, varying from 20 cm to 1 m in width (shown in brown in Fig. 11), but show high strain concentration (Fig. 15A). Within the shear zone, markers such as quartz veins are strongly sheared to boudinaged ribbons or augens (Fig. 15B). On the XZ plane, asymmetric quartz ribbons and augen indicate a south-side-up sense of shear, whereas on the YZ plane boudinaged quartz ribbons show a dextral sense of shear (Fig. 15B). The structural features of these narrow shear zones are consistent with those of the regional late  $D_2$  strike-slip dextral shear zones (Fig. 8). Therefore these narrow shear zones

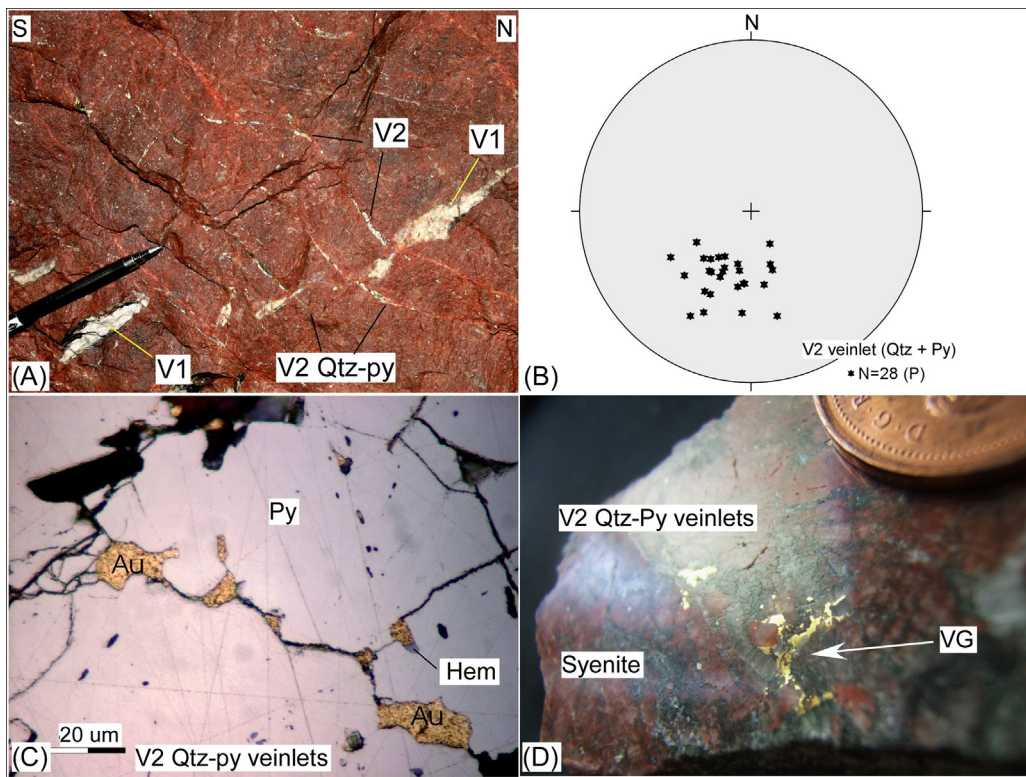


**Fig. 13.** V<sub>2</sub> veins. (A) NE-dipping V<sub>2</sub> Qtz + Py veinlets crosscutting and overprinting V<sub>1</sub> boudinaged veins. (B) Equal-angle lower-hemisphere projection of poles to V<sub>2</sub> veins. (C) Visible gold in V<sub>2</sub> Qtz + Py veinlets in a polished hand specimen. (D) Photomicrograph of a V<sub>2</sub> Qtz + Py veinlet, with free gold along the cracks of or as inclusions within the pyrite.

are correlated with the D<sub>2</sub> deformation. Chlorite–sericite aggregates surround the boudinaged quartz ribbons and form the major foliation of S<sub>2</sub> (Fig. 15B), indicative of a greenschist facies metamorphism, consistent with the regional metamorphic conditions of D<sub>2</sub>.

Apparent crosscutting relationship has shown that the formation V<sub>2</sub> and V<sub>3</sub> veins predate D<sub>2</sub> (Fig. 15A). This interpretation

is further supported by the logging of drill cores, in which V<sub>3</sub> veins are observed to have been folded and crenulated by F<sub>2</sub> folds (Fig. 14E). In summary crosscutting relationships indicate that all V<sub>1</sub> to V<sub>3</sub> veins postdate the emplacement of the Young-Davidson syenite. V<sub>1</sub> veins predate D<sub>1b</sub> deformation, whereas V<sub>2</sub> and V<sub>3</sub> veins are syn-D<sub>1b</sub> and predate the D<sub>2</sub> deformation.

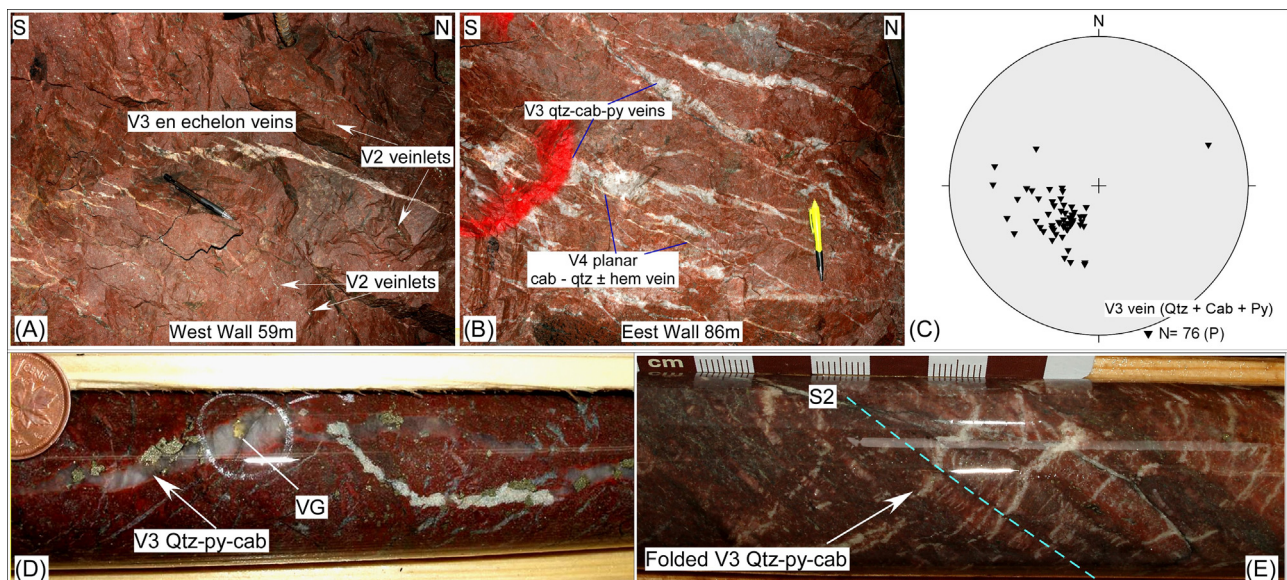


**Fig. 14.** V<sub>3</sub> veins. (A) NE-dipping V<sub>3</sub> Cab + Qtz + Py ± Sch en echelon veins truncating the V<sub>2</sub> veinlets. (B) V<sub>3</sub> en echelon vein arrays overprinted by V<sub>4</sub> planar Cab ± Qtz ± Hem veins. (C) Equal-angle lower-hemisphere projection of poles to V<sub>3</sub> veins. (D) Visible gold associated with V<sub>3</sub> Qtz + Py + Cab planar veins. Note that the host syenite experienced pervasive red hematite–potassium feldspar alteration. (E) V<sub>3</sub> en echelon veins folded by F<sub>2</sub> fold to produce the new S<sub>2</sub> crenulation cleavage, indicative of their formation earlier than D<sub>2</sub>. (For interpretation of the references to color in this figure legend, the reader is referred to the web version of the article.)

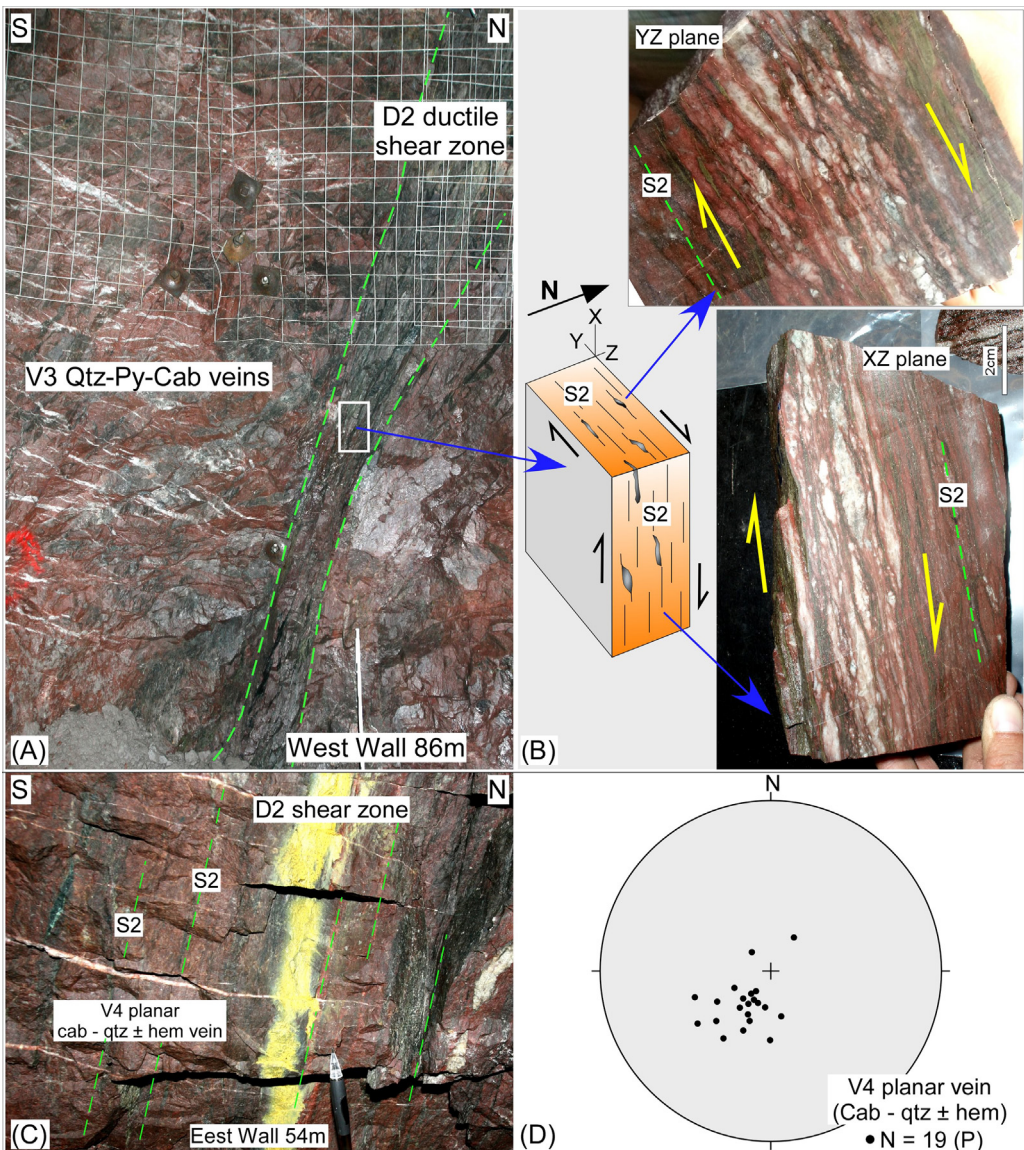


**Fig. 15.** D<sub>2</sub> ductile shear zone and later V<sub>4</sub> veins. (A) V<sub>3</sub> en echelon veins crosscut and truncated by a D<sub>2</sub> ductile shear zone, indicating that the formation of the V<sub>1</sub> to V<sub>3</sub> veins predate the development of the D<sub>2</sub> ductile shear zone. (B) A polished sample from the D<sub>2</sub> shear zone. Asymmetric quartz ribbons and augens indicate a south-side-up sense of shear. (C) V<sub>4</sub> planar Cab + Qtz ± Hem veins truncating and crosscutting S<sub>2</sub> penetrative foliations within the D<sub>2</sub> shear zone. (D) Equal-angle lower-hemisphere projection of poles to V<sub>4</sub> veins.

#### 4.5. V<sub>4</sub> and later veins

V<sub>4</sub> are planar carbonate–quartz±hematite veins that overprint and crosscut all earlier V<sub>1</sub> to V<sub>3</sub> and D<sub>2</sub> ductile shear zones (shown in green in Figs. 11 and 14B). V<sub>4</sub> veins are commonly thin (several millimeters in width), and are characterized by an enrichment of carbonate (up to 90%) comparing to V<sub>1</sub> to V<sub>3</sub> veins (Fig. 15C). V<sub>4</sub> planar veins dip shallowly to the N or NE and have an attitude similar to that of V<sub>2</sub> and V<sub>3</sub> (Fig. 15D). However, overprinting relationships indicate that V<sub>4</sub> veins truncate S<sub>2</sub> foliation and obviously postdate the D<sub>2</sub> deformation (Fig. 15C).

V<sub>4</sub> vein is composed of dominant carbonate and minor quartz and pyrite, and occasionally contains specular hematite. However, the timing, corresponding deformational mechanism and its contributions to the gold mineralization remain unknown.

Very few brittle fault-fill veins vertically crosscut the D<sub>2</sub> shear zones and V<sub>4</sub> planar veins (shown in purple color in Fig. 11). They consist dominantly of pure carbonate with barren sulphide and may

represent a small scale injection of later hydrothermal fluids and are unrelated to the gold mineralization.

#### 5. Discussion and conclusions

##### 5.1. Structures of the Matachewan area: relationships to the CLLDZ

CLLDZ is well known for its spatial association with and controls on world-class gold deposits, such as the Sigma-Lamaque deposit at the Val d'Or area (Table 1; Robert, 1989, 2001a), the Kerr Addison-Chesterville deposit and the Omega deposits at the Larder Lake area (Table 1; Ispolatov et al., 2008). It has been well studied in its middle and eastern sections (Table 1; e.g. Robert, 1989; Desrochers and Hubert, 1996; Wilkinson et al., 1999; Ispolatov et al., 2008), but the western extension of the CLLDZ has received less attention. Although previous studies proposed that the Matachewan area may lay on the CLLDZ, very few structural and kinematic study were

carried out to validate this interpretation (Powell and Hodgson, 1992; Berger and Préfontaine, 2005). In the Matachewan area, there is a large syenite pluton (e.g. Cairo stock) to the east of and a series of small syenite plutons to the north of the Young-Davidson syenite (Fig. 2). However, it is important to note that the gold deposits are spatially associated with those plutons that have experienced multiple generations of folding and shearing deformation (e.g. southern boundary of the Cairo stock and the Young-Davidson syenite; Fig. 2; Berger and Préfontaine, 2005). Therefore, determining the distribution of CLLDZ in the Matachewan area is crucial for understanding the evolution of western part of the CLLDZ and the associated gold mineralization.

The earliest generation of deformation throughout the CLLDZ was interpreted as Pre-Timiskaming deformation that produced a number of upright E-W-trending anticlines and synclines without penetrative axial plane cleavage (Table 1; Dimroth et al., 1983; Bleeker and Parrish, 1996). The following Timiskaming alluvial-fluvial sedimentation occurred unconformably on the early fabrics (Wilkinson et al., 1999 and references therein). However, such the earliest pre-Timiskaming upright folding structures were not observed in the Matachewan area and other segments of the CLLDZ (e.g. eastern part). In this study, the designated D<sub>1a</sub> deformation in the Matachewan area is coeval with the latest phase of Timiskaming sedimentation and syenite emplacement. D<sub>1b</sub> postdates the deposition of Timiskaming assemblage and similar deformational fabrics occur throughout the CLLDZ (defined as D<sub>1</sub> in Robert, 1989; defined as D<sub>2</sub> in Wilkinson et al., 1999; defined as D<sub>2</sub> in Ispolatov et al., 2008; Table 1). The initiation of the nearly E-W-trending CLLDZ is generally considered as the consequence of the D<sub>1</sub> deformation (defined as D<sub>2</sub> in Wilkinson et al., 1999; Ispolatov et al., 2005; Lafrance, 2009; Table 1). In the Matachewan area, D<sub>1</sub> fabric is characterized by significant horizontal shortening, penetrative foliations, steeply plunging stretching lineations, and top-to-N/NE thrust faults, which are consistent with the D<sub>1</sub> fabrics in other parts of the CLLDZ (Table 1). Subsequent D<sub>2</sub> fabric varies from crenulation cleavage to penetrative foliations as approaching the deformation zone (Fig. 6E). D<sub>2</sub> fabrics of the Matachewan area share the largest similarity with other parts of the CLLDZ, which are characterized by steeply plunging F<sub>2</sub> folds, steep L<sub>2</sub> lineations, and dextral shear zones (Figs. 7 and 8; Robert, 1989; defined as the D<sub>3</sub> fabrics in Wilkinson et al., 1999; Table 1). The detailed structural data presented in this study suggest that the Matachewan deformational history and structural interference pattern are similar to other segments of the CLLDZ. Moreover, such interference patterns can be continuously traced from the Matachewan area to the middle segment of the CLLDZ (e.g. Kirkland Lake area; Berger et al., 2006). The Matachewan area therefore represents the western extension of the CLLDZ, which lead us to further convince the previous hypothesis (e.g. Powell and Hodgson, 1992; Berger and Préfontaine, 2005).

## 5.2. Significance of structural setting on ore genesis

Contrasting genetic models for the Young-Davidson gold deposit have been proposed in previous studies, including syn-magmatic models (Sinclair, 1982; Robert, 2001a) and structurally controlled models (Berger and Préfontaine, 2005). Based on the occurrence of disseminated pyrites and stockwork veins, syn-magmatic models suggest that gold mineralization is pre-deformational, and related to the magmatic fluid genetically derived from the cooling syenite intrusion (Sinclair, 1982). Structural mapping on the auriferous veining in the host mafic volcanic rocks (Tisdale assemblage) surrounding the syenite intrusion led to a structural-controlled model that the gold mineralization is genetically correlated to the regional deformation within the CLLDZ, but is controlled by steeply plunging L<sub>2</sub> lineations (same as F<sub>2</sub> fold axis in this study; Berger and Préfontaine, 2005). The most

shortcomings of the previous works and conclusions were largely focused and drawn upon the limited surface outcrops and thus lacked systematic studies on auriferous veining system inside the syenite intrusive body. Detailed 3D structural and petrographic analysis in this study provides rigorous constrains on the setting of the ore genesis and further re-evaluates the pre-existing models.

As demonstrated above, the mineralization zone of the Young-Davidson gold deposit is localized mainly in the syenite intrusion and pinches out in the host mafic volcanic and Timiskaming sedimentary rocks (Fig. 10). This observation indicates that the syenite itself may largely control the gold mineralization. This interpretation is consistent with the outcrop-scale detailed mapping on the Young-Davidson mine site (Fig. 16; outcrop location shown in Fig. 10). As shown in Fig. 16, the syenite dyke intrudes into the Timiskaming sandstone and crosscuts the pre-titled beddings (also see Fig. 4B). Meanwhile both syenite and host sandstone are overprinted by the S<sub>1b</sub> foliation, indicating that the syenite dyke is a syn-D<sub>1</sub> intrusion. Numerous quartz-carbonate vein arrays show preferred N or NE-dipping orientation developing mostly within the syenite. By contrast, very few veins develop in the host sandstone except along the semi-brITTLE fold hinge area in which the sandstone is much more competent for the injection of the hydrothermal veins (Fig. 16). This interpretation is further supported by the representative deposit-scale cross section (Fig. 17, location refers to Fig. 10). As shown in Fig. 17, the syenite intruded into the lithological contact between the Tisdale mafic volcanic and Timiskaming sedimentary rocks, all of which are overprinted by the CLLDZ. The gold ore body is a linear mineralization zone that is mostly developed in the syenite intrusion and partly in the surrounding Timiskaming sedimentary rocks (Fig. 17). All these indicate that the syenite of the Young-Davidson deposit acts as a competent host and controls the distribution of the hydrothermal veins.

Our detailed mapping results have revealed that the Young-Davidson syenite intrusion is located on the margin of the CLLDZ (Fig. 2). Each generation of the veins within the syenite show preferred orientation corresponding to a specific generation of regional deformation, suggesting that they were formed and controlled under a specific stress field related to the development of the CLLDZ. The competent nature, ductile to semi-brITTLE structures, numerous fault systems, focus of heterogeneous strain, multiple stages of hydrothermal activities therefore make the syenite an ideal mechanical trap for the Young-Davidson gold mineralization.

In the Young-Davidson syenite intrusion, detailed structural and petrographic analysis reveals four generations of veins (V<sub>1</sub>–V<sub>4</sub>). Their geometry, mutual overprinting relationship and correlation to the regional structures are all synthesized in a block diagram (Fig. 18). V<sub>1</sub> ankerite-pyrite-quartz veins have been intensely folded, boudinaged and displaced by the D<sub>1b</sub> thrust faults. Its formation postdates the emplacement of the syenite and predates the D<sub>1b</sub> deformation. However, its relation to the gold mineralization remains unclear due to intense overprinting by the following V<sub>2</sub> and V<sub>3</sub> veins. V<sub>2</sub> quartz-pyrite veinlets postdate V<sub>1</sub> veins and predate D<sub>1b</sub> thrust faults. The preferred NE-dipping orientation and sigmoidal to en echelon vein geometry indicate that it is structurally controlled and formed under a relatively stable compressional environment with dip-slip shearing component (Fig. 18). V<sub>3</sub> quartz-carbonate-pyrite en echelon veins postdate V<sub>2</sub> veins and are synchronous with the top-to-NE D<sub>1b</sub> thrusting deformation. Petrographic data have revealed that gold mineralization is mainly associated with V<sub>2</sub> and partially with V<sub>3</sub>, both of which occur synchronously with the development of the regional D<sub>1b</sub> deformation within the CLLDZ. The high strain CLLDZ may have served as a conduit for gold-bearing hydrothermal fluids. The gold mineralization within the Young-Davidson syenite therefore largely favors a structurally-controlled model (e.g. Berger and

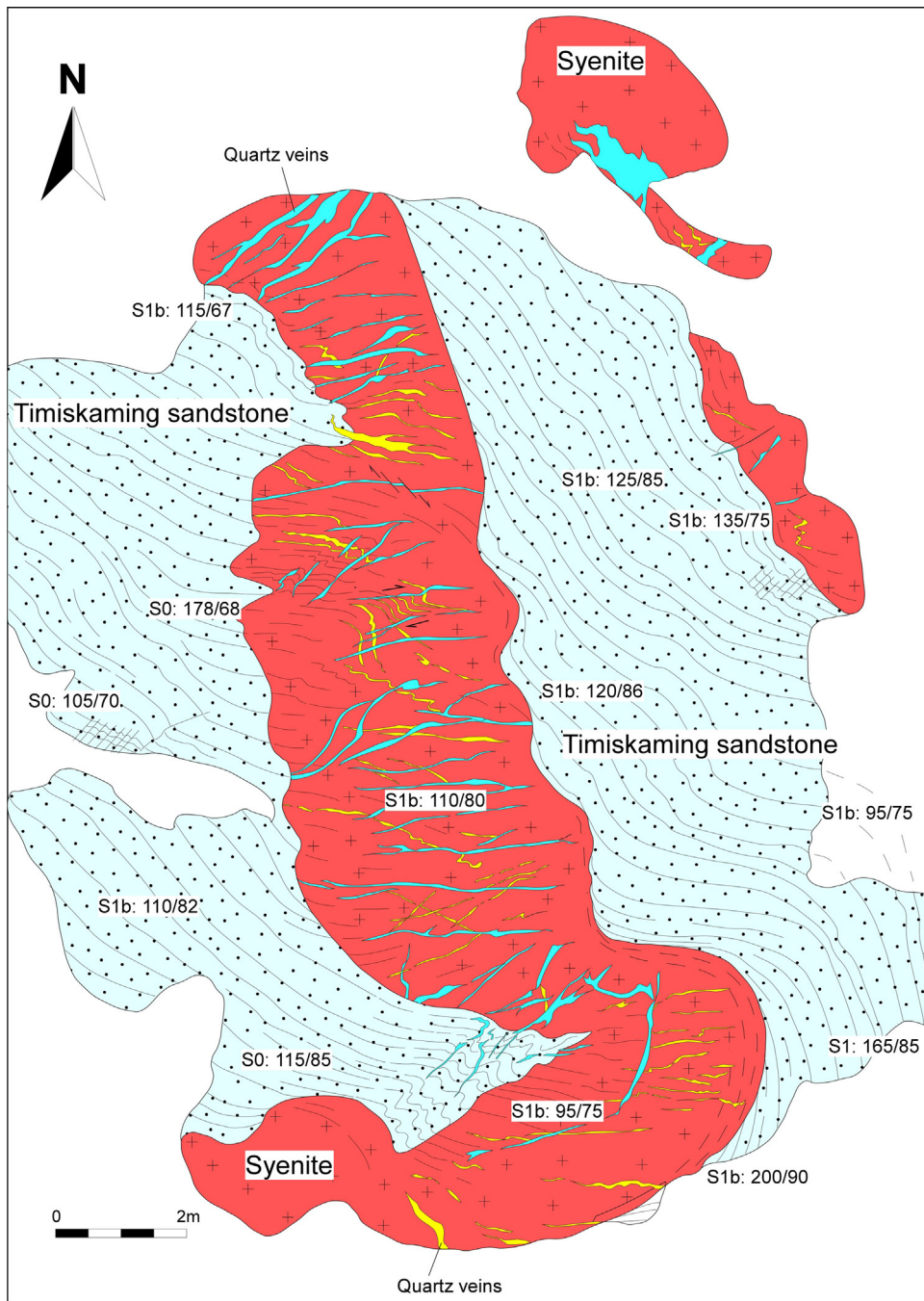


**Fig. 16.** Detailed outcrop-scale structural map showing competency contrast between syenite intrusion and the host Timiskaming sedimentary rocks. Concentration of quartz veins within the syenite indicating it as a competent host for the gold mineralization. Outcrop location is shown in Fig. 10.

Préfontaine, 2005) rather than a syn-magmatic model (Sinclair, 1982). Progressive shortening triggers the top-to-N/NE shear component that leads to the opening of  $V_2$  and  $V_3$  veins, along which hydrothermal fluids inject into the tension gaps and deposit to form the Young-Davidson gold deposit. A systematic channel sampling and gold assay along the No.9 ore crosscut done by the Northgate Minerals Corporation. Gold assay results are shown on [Inline Supplementary Fig. 1](#). A comparison between gold grade and veining distribution shows that the enrichment of gold largely controlled by the abundance of the  $V_2$  and  $V_3$  veins. The gold mineralization is therefore controlled by  $V_2$  and  $V_3$  veins, not the  $L_2$  lineations as previously considered (e.g. Berger and Préfontaine,

2005). The Young-Davidson syenite intrusion is acting as a competent structural trap for the gold mineralization (Fig. 16). The following E-W-trending  $D_2$  shear zone probably marks the end of the main stage of vein-hosted gold mineralization of the Young-Davidson deposit, although contribution of the youngest  $V_4$  veins remains uncertain. A proportion of the gold mineralization at Young-Davidson is also associated with disseminated and relatively high temperature potassic alteration (Martin, 2012; Naderi, 2013). The timing of the precipitation of disseminated pyrite and potassic alteration, also likely to have  $D_{1b}$  timing (Naderi, 2013). Further petrological and geochemical studies are demanded to resolve this issue.

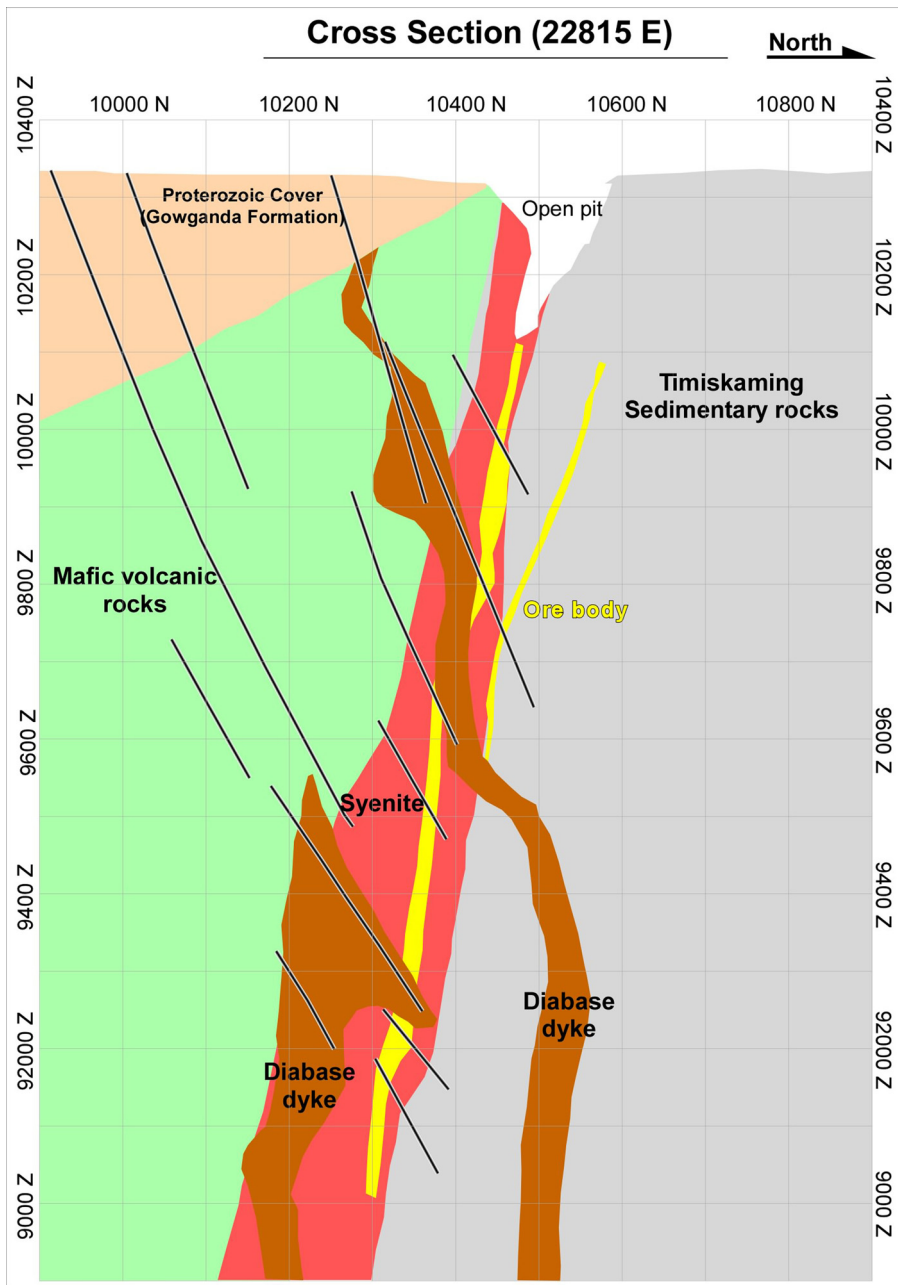


**Fig. 17.** Representative deposit-scale cross section showing the distribution of the ore body in both syenite and surrounding Timiskaming sedimentary rocks. Refer to Fig. 10 for the cross section location (modified after the cross section E22815, AuRico Gold Inc.).

### 5.3. Conclusions

The major conclusions of this paper are:

- (1) The multiply deformed Matachewan area experienced four generations ( $D_1$ – $D_4$ ) of deformation.  $D_{1a}$  records a NE-SW-oriented shortening and resulted in regional upright folding without penetrative foliations. Its development is coeval with the latest phase of Timiskaming sedimentation and syenite emplacement. Subsequent  $D_{1b}$  is resulted from progressively NE-SW-oriented shortening and generates regional penetrative foliations and a series of top-to-NE reverse faults.  $D_2$  occurs during a NW-SE-oriented shortening and produces asymmetric folds, oblique-slip thrusts and dextral strike-slip shear zones.  $D_3$  semi-brittle refolds the earlier fabrics, whereas the latest  $D_4$  sinistral fault records a Paleoproterozoic brittle

deformation. The superposition of  $D_1$  and  $D_2$  fabrics largely defines the pattern of the nearly E-W trending high strain zone in the Matachewan area. Deformational features and structural interference patterns of the linear high strain zone show large consistency with those of and can be continuously traced to the middle segment of the CLLDZ. The Matachewan area is therefore the western extension of the CLLDZ.

- (2) The Young-Davidson syenite intrusion is located at the margin of the CLLDZ. It is a syn- $D_1$  intrusion. Four generations of veins ( $V_1$ – $V_4$ ) are developed after the emplacement of the intrusion.  $V_1$  folded and boudinaged quartz–ankerite veins occur earlier than and are crosscut by the  $D_{1b}$  fabrics.  $V_2$  veins are represented by folded quartz–pyrite veinlets,  $V_3$  veins are comprised of en echelon quartz–carbonate veins with sulfide minerals. Main stage of gold mineralization within the syenite is associated with the development of  $V_2$  veinlets and partly  $V_3$  veins,

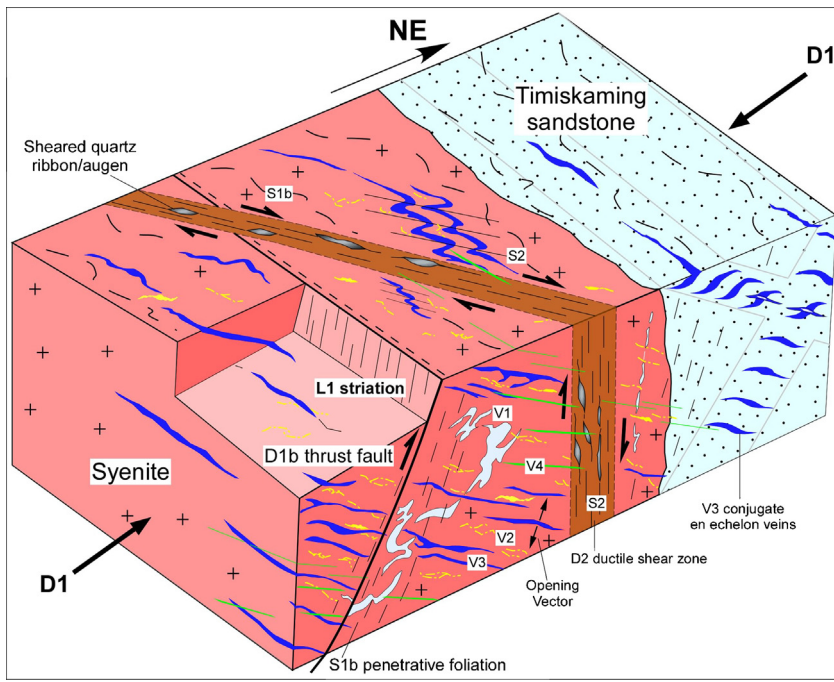


**Fig. 18.** Block diagram showing the spatial and overprinting relationships between different stages of veins and regional structures.

which are opened during the D<sub>1b</sub> NE-SW-oriented shortening and associated top-to-N/NE shearing deformational event. V<sub>4</sub> planar carbonate-quartz veins postdate the D<sub>2</sub> deformation and represent the latest veins of the intrusion. Young-Davidson gold deposit is a mostly structurally controlled lode-gold deposit and the hosting syenite is served as a competent structural trap for gold mineralization.

## Acknowledgements

This research was supported by a Collaborative Research and Development Grant, Natural Sciences and Engineering Research Council of Canada grant to Robert Linnen and Shoufa Lin. Comments by Yvette Kuiper and an anonymous reviewer led to significant improvement to the manuscript and are greatly appreciated. We are very grateful for the generous financial, logistical and technical support provided by Northgate Minerals and AuRico Gold Inc. In particular we would like to thank Carl Edmunds, Jim Janzen and Chris Rockingham.

## References

- Ayer, J., Amelin, Y., Corfu, F., Kamo, S., Ketchum, J., Kwok, K., Trowell, N., 2002. Evolution of the southern Abitibi greenstone belt based on U-Pb geochronology; autochthonous volcanic construction followed by plutonism, regional deformation and sedimentation. *Precambrian Research* 115, 63–95.
- Ayer, J.A., Thurston, P.C., Bateman, R., Dubé, B., Gibson, H.L., Hamilton, M.A., Hathaway, B., Hocker, S.M., Houle, M.G., Hudak, G., Ispolatov, V.O., Lafrance, B., Lesser, C.M., MacDonald, P.J., Peloquin, A.S., Piercey, S.J., Reed, L.E., Thompson, P.H., 2005. Overview of results from the Greenstone Architecture Project: Discover Abitibi Initiative. In: Ontario Geological Survey, Open File Report 6154, pp. 146.
- Berger, B.R., Préfontaine, S., 2005. General geology of Powell Township, District of Timiskaming. In: Baker, C.L., Debicki, E.J., Kelly, R.I., Ayer, J.A., Easton, R.M., Madon, Z.B. (Eds.), Summary of Field Work and Other Activities 2005, Ontario Geological Survey, Open File Report 6172, pp. 5–1–5–10.
- Berger, B.R., 2006. Geological synthesis along Highway 66 from Matachewan to Swastika. Ontario Geological Survey, Open File Report 6177, 125 pp.
- Berger, B.R., Pigeon, L., Leblanc, G., 2006. Precambrian geology, Highway 66 area, Swastika to Matachewan. Ontario Geological Survey, Map 2677, Scale 1:50,000.
- Bleeker, W., Parrish, R.R., 1996. Stratigraphy and U-Pb zircon geochronology of Kidd Creek: implications for the formation of giant volcanogenic massive sulfide deposits and the tectonic history of the Abitibi greenstone belt. *Canadian Journal of Earth Sciences* 33, 1213–1231.
- Card, K.D., Poulsen, K.H., Robert, F., 1989. The Archean Superior Province of the Canadian Shield and its lode gold deposits. In: Keays, R.R., Ramsay, W.R.H., Groves, D.I. (Eds.), The Geology of Gold Deposits: The Perspective in 1988: Economic Geology Monograph 6, pp. 19–36.
- Card, K.D., 1990. A review of the Superior Province of the Canadian Shield, a product of Archean accretion. *Precambrian Research* 48, 99–156.
- Colvane, A.C., 1989. An empirical model for the formation of Archean gold deposits: products of final cratonization of the Superior Province, Canada. In: Keays, R.R., Ramsay, W.R.H., Groves, D.I. (Eds.), The Geology of Gold Deposits: The Perspective in 1988: Economic Geology Monograph 6, pp. 37–53.
- Corfu, F., 1993. The evolution of the southern Abitibi greenstone belt in light of precise U-Pb geochronology. *Economic Geology* 88, 1323–1340.
- Desrochers, J.-P., Hubert, C., 1996. Structural evolution and early accretion of the Archean Malartic composite block, southern Abitibi greenstone belt, Quebec, Canada. *Canadian Journal of Earth Sciences* 33, 1556–1569, <http://dx.doi.org/10.1139/e96-118>.
- Dimroth, E., Imreh, L., Goulet, N., Rocheleau, M., 1983. Evolution of the south-central segment of the Archean Abitibi Belt, Quebec. Part II: tectonic evolution and geomechanical model. *Canadian Journal of Earth Sciences* 20, 1355–1373.
- Hamilton, J.V., Hodgson, C.J., 1984. Structural geology and gold mineralization in the Kirkland Lake-Larder Lake deformation zone. In: Ontario Geological Survey, Miscellaneous Paper 119, pp. 220–225.
- Heaman, L.M., 1997. Global mafic magmatism at 2.45 Ga: remnants of an ancient large igneous province? *Geology* 25, 299–302.
- Hodgson, C.J., Hamilton, J.V., 1989. Gold mineralization in the Abitibi Greenstone Belt: End-stage result of Archean collisional tectonics? In: Keays, R.R., Ramsay, W.R.H., Groves, D.I. (Eds.), The Geology of Gold Deposits: The Perspective in 1988: Economic Geology Monograph 6, pp. 86–100.
- Hodgson, C.J., Hamilton, J.V., Guimond, R.P., 1991. Relationship between gold deposits and the tectonic framework of the Abitibi greenstone belt in the Kirkland Lake-Larder Lake area. Ontario Geological Survey, Open File Report 5782.
- Ispolatov, V., Lafrance, B., Dubé, B., Hamilton, M., Creaser, R., 2005. Geology, structure, and gold mineralization, Kirkland Lake and Larder Lake areas (Gauthier and Teck townships): Discover Abitibi Initiative. Ontario Geological Survey, Open File Report 6159, 170 pp.
- Ispolatov, V., Lafrance, B., Dubé, B., Creaser, R., Hamilton, M., 2008. Geologic and structural setting of gold mineralization in the Kirkland Lake-Larder Lake Gold Belt, Ontario. *Economic Geology* 103, 1309–1340.
- Lafrance, B., 2009. Is the Larder Lake – Cadillac Deformation Zone a Transpression Zone? Eos, Transactions, American Geophysical Union 90(22) (Jt. Assem. Suppl., Abstract GA22A-05).
- Linnen, R.L., Lin, S., Zhang, J., Martin, R.D., Naderi, N., Davis, D.W., Hamilton, M.A., Creaser, R.A., Berger, B.R., Banerjee, N.R., Wing, B.A., Wu, C., 2012. Section 3: A synthesis of the structure, petrology, geochronology and geochemistry of the Young-Davidson gold deposit and surrounding area. Report in Results from the Shining Tree, Chester Township and Matachewan Gold Projects and the Northern Cobalt Embayment Polymetallic Vein Project, Ontario Geological Survey, Miscellaneous Release—Data 294.
- Lovell, H.L., 1967. *Geology of the Matachewan area; Ontario Department of Mines. Geological Report 51*, 61 pp.

- Ludden, J., Hubert, C., Gariépy, C., 1986. The tectonic evolution of the Abitibi greenstone belt of Canada. *Geological Magazine* 123, 153–166.
- Martin, R., 2012. Syenite-hosted gold mineralization and hydrothermal alteration at the Young-Davidson deposit, Matachewan, Ontario. Master Thesis of the University of Waterloo, 172 pp.
- Mason, R., Helmstaedt, H.H., 1992. Structural controls during formation and deformation of Archean lode-gold deposits in the Canadian Shield. In: Bartholomew, M.J., Hyndman, D.W., Mogk, D.W., Mason, R. (Eds.), *Basement Tectonics 8: Characterization and Comparison of Ancient and Mesozoic Continental Margins*. Proceedings of the 8th International Conference on Basement Tectonics. Butte, Montana, 1988. Kluwer Academic Press, Dordrecht, pp. 625–631.
- Mueller, W., Donaldson, J.A., Doucet, P., 1994. Volcanic and tectono-plutonic influence on sedimentation in the Archean Kirkland Basin, Abitibi greenstone belt, Canada. *Precambrian Research* 68, 201–230.
- Naderi, N., 2013. Stable Isotopes and XRD Investigation of Gold Mineralization at the Syenite-Hosted Young-Davidson Deposit, Matachewan, Ontario. MSc. University of Western Ontario, 159 pp.
- Olivo, G.R., Chang, F., Kyser, T.S., 2006. Formation of the Auriferous and Barren North Dipper Veins in the Sigma Mine, Val d'Or, Canada: Constraints from Structural, Mineralogical, Fluid Inclusion, and Isotopic Data. *Economic Geology* 101, 607–631.
- Poulsen, K.H., Card, K.D., Franklin, J.M., 1992. Archean tectonic and metallogenic evolution of the superior province of the Canadian shield. *Precambrian Research* 58, 25–54.
- Poulsen, K.H., Robert, F., Dube, B., 2000. Geological classification of Canadian gold deposits. *Geological Survey of Canada Bulletin* 540, 106.
- Powell, W.G., 1991. The distribution, structural history and relationship to regional metamorphism of high-strain zone forming the Larder Lake–Cadillac Deformation Zone, Matachewan Area, Abitibi belt. Ontario Geological Survey, Open File Report 5789, 150 pp.
- Powell, W.G., Hodgson, C.J., 1992. Deformation of the Gowganda Formation, Matachewan area, Ontario, by post-Early Proterozoic reactivation of the Archean Larder Lake – Cadillac break, with implications for gold exploration. *Canadian Journal of Earth Sciences* 29, 1580–1589.
- Robert, F., 1989. Internal structure of the Cadillac tectonic zone southeast of Val d'Or, Abitibi greenstone belt, Québec. *Canadian Journal of Earth Sciences* 26, 2661–2675.
- Robert, F., 2001a. Syenite-associated disseminated gold deposits in the Abitibi greenstone belt, Canada. *Mineralium Deposita* 36, 503–516.
- Robert, F., 2001b. Vein Formation and Deformation in Greenstone Gold Deposits. *Society of Economic Geologists Reviews* 14, 111–155.
- Sinclair, W.D., 1982. Gold deposits of the Matachewan Area, Ontario. In: Hodder, R.W., Petruk, W. (Eds.), *Geology of Canadian Gold Deposits*. Canadian Institute of Mining and Metallurgy, Special Volume 24, 83–93.
- Smith, J.P., Spooner, E.T.C., Broughton, D.W., Ploeger, F.R., 1993. Archean Au-Ag-(W) quartz vein/disseminated mineralisation within the Larder Lake–Cadillac Break, Kerr Addison–Chesterville System, Northeast Ontario, Canada. Ontario Geological Survey Open File Report 5831, 310 pp.
- Toogood, D.J., Hodgson, C.J., 1985. A structural investigation between the Kirkland Lake and Larder Lake gold camps. In: Ontario Geological Survey, Miscellaneous Paper 127, pp. 200–205.
- Wilkinson, L., Cruden, A.R., Krogh, T.E., 1999. Timing and kinematics of post-Timiskaming deformation within the Larder Lake–Cadillac deformation zone, southwest Abitibi greenstone belt, Ontario, Canada. *Canadian Journal of Earth Sciences* 36, 627–647.